ACS Infectious Diseases

Article

Antiplasmodial mode of action of pantothenamides: pantothenate kinase serves as a metabolic activator, not as a target

Marianne de Villiers, Christina Spry, Cristiano Joao Macuamule, Leanne Barnard, Gordon Wells, Kevin J Saliba, and Erick Strauss

ACS Infect. Dis., **Just Accepted Manuscript** • Publication Date (Web): 24 Apr 2017

Just Accepted

ACS Publications

ACS Infectious Diseases is published by the American Chemical Society. 1155 Sixteenth Street N.W., Washington, DC 20036

Antiplasmodial mode of action of pantothenamides: pantothenate kinase serves as a metabolic activator, not as a target

Marianne de Villiers[†]*, Christina Spry[‡], Cristiano J. Macuamule[†], Leanne Barnard[†], Gordon Wells[†], Kevin J. Saliba[‡,§] and Erick Strauss[†]*

[†]Department of Biochemistry, Stellenbosch University, Stellenbosch, 7600, South Africa.
[‡]Research School of Biology, and [§]Medical School, College of Medicine, Biology and Environment, The Australian National University, Canberra, Australian Capital Territory, 2601, Australia.

*To whom correspondence should be addressed: mdevilliers@sun.ac.za; estrauss@sun.ac.za

ABSTRACT

N-substituted pantothenamides (PanAms) are pantothenate analogues with up to nanomolar potency against blood-stage *Plasmodium falciparum* (the most virulent species responsible for malaria). Although these compounds are known to target coenzyme A (CoA) biosynthesis and/or utilization, their exact mode of action (MoA) is still unknown. Importantly, PanAms that retain the natural β-alanine moiety are more potent than other variants, consistent with the involvement of processes that are selective for pantothenate (the precursor of CoA) or its derivatives. The transport of pantothenate and its phosphorylation by *P. falciparum* pantothenate kinase (*Pf*PanK, the first enzyme of CoA biosynthesis) are two such processes previously highlighted as potential targets for the PanAms' antiplasmodial action. In this study, we investigated the effect of PanAms on these processes using their radiolabeled versions (synthesized here for the first time), which made possible the direct measurement of PanAm uptake by isolated blood-stage parasites, and PanAm phosphorylation by *Pf*PanK present in parasites lysates. We found that the MoA of PanAms does not involve interference with pantothenate transport, and that inhibition of *Pf*PanK-mediated pantothenate phosphorylation does not correlate with PanAm antiplasmodial activity. Instead, PanAms that retain the β-alanine moiety were found to be metabolically activated by *Pf*PanK in a selective manner, forming phosphorylated products that likely inhibit other steps in CoA biosynthesis, or are transformed into CoA antimetabolites that can interfere with CoA utilization. These findings provide direction for the ongoing development of CoA-targeted inhibitors as antiplasmodial agents with clinical potential.

Keywords

Coenzyme A biosynthesis, antimicrobial, antimetabolite, pantothenamide, pantothenate uptake.

INTRODUCTION

N-substituted pantothenamides (PanAms) are analogues of pantothenate (Pan), the precursor of the essential metabolic cofactor coenzyme A (CoA) (Figure 1a). These compounds inhibit the proliferation of blood-stage *Plasmodium falciparum*,[1-5] the parasite responsible for most of the deaths attributed to malaria.[6] In fact, the most potent antiplasmodial member of the class identified to date—*N*-phenethyl-pantothenamide (*N*-PE-PanAm)—has a potency comparable to that of chloroquine (IC_{50}, i.e. the concentration that gives half-maximal inhibition, of ~20 nM).[4] However, PanAms are sensitive to degradation by pantetheinase, a serum enzyme that belongs to the Vanin protein family,[7-8] and their potency is therefore considerably reduced unless this enzyme is inactivated.[4,9] We previously demonstrated that exchanging the β-alanine moiety of the PanAm structure with either glycine or γ-aminobutyric acid (yielding α-PanAms and HoPanAms respectively; the "normal", unmodified structures are referred to as *n*-PanAms) reduces degradation significantly (Figure 1b).[5] However, this change also reduces the potency of the best of the molecules, suggesting that the β-alanine moiety is required for the PanAms' mode of action (MoA).[2]

The finding that addition of Pan reverses the antiplasmodial effect of the PanAms,[2,4-5] indicates that these compounds target processes involved in Pan utilization (i.e. its uptake and biosynthetic conversion to CoA) and/or processes that require CoA or its thioesters.[10] However, the exact antiplasmodial MoA of the PanAms remains unknown. Four possible MoAs have been proposed, as shown in Figure 1a.[11] Among these possibilities, *Pf*PanK has long been considered a strong candidate for the target of PanAm-mediated antiplasmodial activity. Indeed, Pan is the only vitamin that is required for survival of blood-stage *P. falciparum*[12] (thiamine becomes essential only after extensive depletion from erythrocytes[13]), and its phosphorylation by *Pf*PanK allows the parasite to compete for the vitamin with its human host.[14] However, the activity of *Pf*PanK has only been studied in lysates (due to a failure to date to express the enzyme heterologously[15]) using an assay that tracks the phosphorylation of radiolabeled substrates.[4,14,16-20] These reports indicated that *Pf*PanK has a submicromolar K_M for Pan, and that its ability to phosphorylate Pan is potently inhibited by certain PanAms (and other Pan analogues), especially those with hydrophobic substituents. However, the relevance of these data to the MoA of the PanAms has thus far remained unclear.

In contrast, the importance of PanK to the MoA of the PanAms in bacteria has been explored in more detail,[21-25] partly because prokaryotes have been shown to have three different types of PanK.[26] These types differ in regards to structure, activity profiles and the level of substrate specificity, providing an ideal tool for the study of PanK's involvement in PanAm

inhibition in these organisms.[11] The studies demonstrated that in organisms (such as *Escherichia coli*) that have non-selective type I PanKs, the enzyme acts as a metabolic activator that initiates the transformation of the PanAms (including its α-PanAm and HoPanAm variants[27]) into CoA antimetabolites,[28-29] lowering CoA levels and inhibiting CoA-dependent processes[22-24,30-31]—including fatty acid biosynthesis, which is dependent on CoA for activation of the *apo*-acyl carrier protein (ACP) of the type II fatty acid synthase to its active *holo*-form.[32] In contrast, organisms that have highly selective type III PanKs are completely resistant to inhibition by the PanAms, as these enzymes do not recognize them as substrates and therefore they are not metabolically activated. However, between these extremes is at least one example—*Staphylococcus aureus*—in which PanAm-mediated growth inhibition occurs at least partially through direct inhibition of the target organism's PanK.[27] The *S. aureus* PanK (*Sa*PanK) is an atypical type II PanK that shows high specificity for Pan and the *n*-PanAms, accepting the latter as substrates.[22] Recently, it was shown that the phosphorylated products get trapped on the enzyme, leading to its inhibition *in vitro*.[33] Due to the enzyme's specificity, the α-PanAms and HoPanAms do not inhibit *Sa*PanK and show no inhibition of *S. aureus* growth.[27]

Taken together, these previous studies indicate that to gain a better understanding of *Pf*PanK's role in PanAm inhibition of *P. falciparum*—including the requirement of the β-alanine moiety for the maintenance of these molecules' potency—a more in-depth study of the kinetics and specificity of the parasite enzyme is required. Furthermore, since *P. falciparum* is highly dependent on Pan, the selective inhibition of the uptake of the vitamin by the parasite's Pan transporter presents an additional potential vulnerability that could also introduce the observed structural selectivity filter. Yet no studies have been performed on the susceptibility of Pan uptake to inhibition by the PanAms to date.

In this study we set out to investigate the basis for the PanAms' specificity profile in *P. falciparum*, and shed light on their antiplasmodial MoA. This was achieved through the use of various PanAm variants and their analogues (including radiolabeled versions) in uptake studies and in phosphorylation assays using parasite lysates. Our results show that the PanAm MoA does not depend on the inhibition of Pan uptake or *Pf*PanK activity. Instead, *Pf*PanK acts as a highly specific metabolic activator of the PanAms. This study provides clear direction for the future development of different variants of the PanAms as antiplasmodial agents based on a suggested MoA that depends on the inhibition of a target beyond PanK.

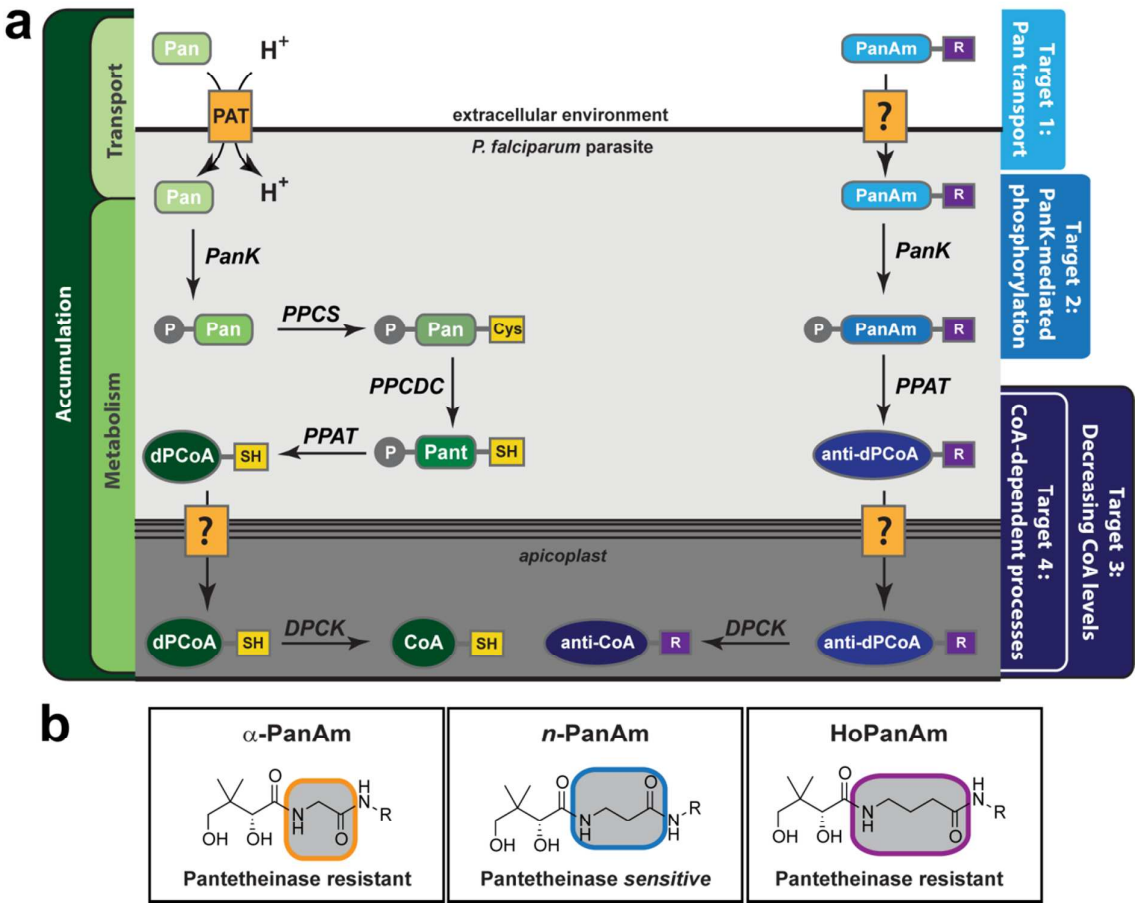

Figure 1. a) Biosynthesis of CoA in *P. falciparum*. Uptake of pantothenate (Pan) is followed by its biosynthetic conversion to CoA in a five-step pathway catalyzed by pantothenate kinase (PanK), phosphopantothenoylcysteine synthetase (PPCS), phosphopantothenoylcysteine decarboxylase (PPCDC), phosphopantetheine adenylyltransferase (PPAT), and finally dephospho-CoA kinase (DPCK), that produce 4'-phosphopantothenate (P-Pan), 4'-phosphopantothenoylcysteine (P-PanCys), 4'-phosphopantetheine (P-PantSH), 3'-dephospho-CoA (dPCoA) and CoA, respectively. The accumulation of Pan can be represented by the combined effects of the transport of the vitamin into the parasite and its metabolism by the CoA pathway starting with PanK-mediated phosphorylation. This ultimately leads to trapping of Pan within the parasite. Pantothenamides (shown as PanAm–R in the figure, with R denoting the amide substituent) can also be taken up by the parasite to exert their effect on CoA biosynthesis and/or utilization. PanAms are proposed to exert an antiplasmodial effect via one of four possible processes, or a combination thereof: 1) by inhibiting Pan transport, 2) by inhibiting PanK-mediated Pan phosphorylation, 3) by lowering CoA levels due to formation of CoA antimetabolites (anti-CoA) rather than CoA, and 4) by CoA antimetabolites interfering with CoA-dependent processes. **b)** PanAms that contain a β-alanine moiety (i.e. *n*-PanAms, middle) are susceptible to degradation by pantetheinase. Modification of the β-alanine moiety that displaces the scissile bond produces the α-PanAm (left) or HoPanAm (right) variants that are resistant to pantetheinase.[5]

RESULTS AND DISCUSSION

Investigating the impact of PanAm variants on Pan accumulation in isolated *P. falciparum* parasites. We first determined whether the PanAms have an impact on the accumulation of Pan (i.e. the combination of transport of extracellular Pan across the parasite plasma membrane and its metabolism by the enzymes of the CoA biosynthesis pathway, see Figure 1a) in intact *P. falciparum* parasites. This was achieved by measuring the uptake of radiolabeled Pan by isolated parasites[14] in the presence of two different *n*-PanAms—*N*-pentyl pantothenamide (N5-Pan) and *N*-PE-PanAm—that showed good antiplasmodial activity in a previous study.[5] The α-PanAm and HoPanAm counterparts of these compounds were also tested to determine if the observed selectivity for the β-alanine moiety of the *n*-PanAms could be related to the accumulation process.

Intact trophozoite-stage *P. falciparum* parasites were isolated by saponin-mediated permeabilization of the erythrocytic membranes and accumulation of [^{14}C]Pan was measured in the presence of increasing concentrations of the various PanAms after 20 minutes (i.e. within the linear phase of accumulation). The accumulation was found to be inhibited by the PanAms in a dose-dependent manner (Figure 2a and b). The IC_{50} values calculated from the corresponding dose response curves indicated that while all the PanAms tested showed inhibition, the *n*-PanAm and HoPan variants (with either of the tested substituents) are more potent than their α-PanAm counterparts (Table 1, left). This finding correlates with the antiplasmodial potency of these compounds, suggesting that the observed selectivity is based on one of the processes involved in accumulation (Figure 2c). In addition, we found that the [^{14}C]Pan distribution ratio (i.e. the ratio of [^{14}C]Pan inside the cell to that in the extracellular solution) reached a value of approximately one as the PanAm concentrations were increased. This value indicates that in the presence of the PanAms the compound continues to equilibrate across the parasite membrane but that little to no metabolism takes place. These results are consistent with the PanAms having a negative impact on the metabolism, rather than the uptake, of the vitamin (Figure 2a and b).

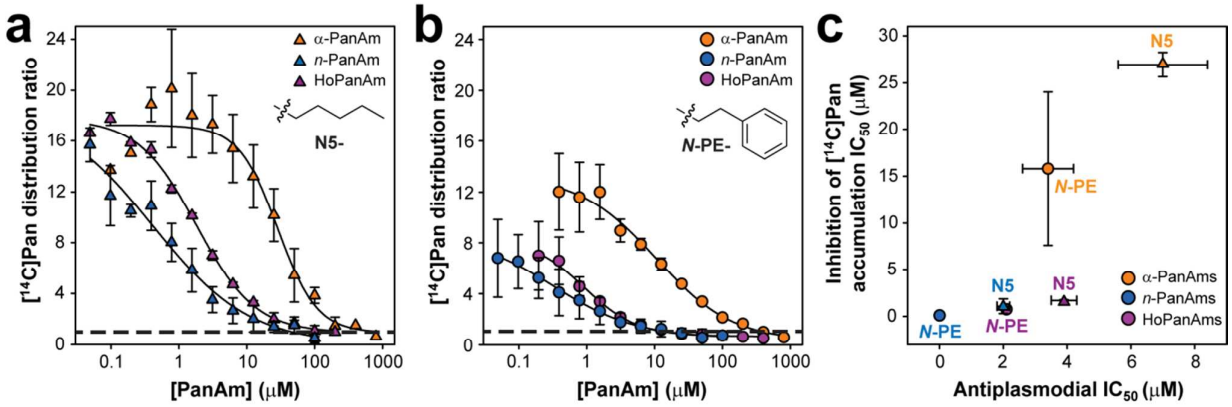

Figure 2. Effect of α-, *n*- and HoPanAms (N5 series in panel **a** and *N*-PE series in panel **b**, respectively) on [^{14}C]Pan accumulation (the combined effect of transport and metabolism) as measured by saponin-isolated *P. falciparum* trophozoites after 20 minutes. Accumulation decreases with increasing concentrations of the PanAms and reaches a distribution ratio of approximately one (indicated by a black dashed line). Accumulation data are an average of two separate experiments, each performed in duplicate. All error bars denote range/2. **c)** Correlation of the potency of inhibition of [^{14}C]Pan accumulation in isolated *P. falciparum* trophozoites by PanAms and the antiplasmodial potency obtained for PanAms against cultured blood-stage *P. falciparum* parasites. Antiplasmodial IC_{50} values were obtained from previous studies.[4-5] Error bars denote SEM or range/2 as appropriate for the particular data set.

Table 1. Inhibition of the accumulation of radiolabeled Pan or PanAms in isolated *P. falciparum* parasites by non-labeled substrates.

Inhibition of accumulation of [^{14}C]Pan by indicated PanAms			Inhibition of accumulation of indicated [^{14}C]PanAms by Pan		
Non-labeled inhibitor variant	IC_{50} (μM)[a]		Radiolabeled substrate variant	IC_{50} (μM)[a]	
	N5 series	*N*-PE series		N6 series	*N*-Bn series
α-PanAm	27 ± 1	16 ± 8	α-PanAm	0.87 ± 0.01	0.64 ± 0.09
n-PanAm	1.1 ± 0.8	0.11 ± 0.06	*n*-PanAm	44 ± 21	18 ± 2
HoPanAm	1.7 ± 0.1	0.76 ± 0.07	HoPanAm	6.8 ± 2.6	7.0 ± 0.7

[a]The IC_{50} of PanAm-mediated inhibition of [^{14}C]Pan accumulation (on the left) and Pan-mediated inhibition of [^{14}C]PanAm accumulation (on the right) in intact isolated trophozoite-stage parasites after a 20 minute incubation at 37 ºC. The reported values represent the averages of two independent experiments each performed in duplicate; the errors indicate the range/2.

Synthesis of two sets of radiolabeled PanAms provides suitable tool and control compounds for studying their uptake and metabolism in *P. falciparum*. More detailed investigations into the uptake and metabolism of PanAms by saponin-isolated parasites required the synthesis of radiolabeled PanAms. Consequently, we performed the first synthesis of radiolabeled PanAms described to date by modification of a previously developed method.[34]

Two sets of PanAm variants—one based on N6-PanAm that shows good antiplasmodial activity[5], and another based on *N*-Bn-PanAm that is inactive[4]—were prepared for this study using [^{14}C]hexylamine and [^{14}C]benzylamine, two radiolabeled amines that are commercially available. We included the inactive compound specifically to act as control, i.e. with the expectation that they should show behavior distinct from their antiplasmodial counterparts. With the compounds in hand, we turned to performing accumulation experiments as described for [^{14}C]Pan above.

The accumulation of PanAms in isolated *P. falciparum* parasites points to an effect related to metabolism, not uptake. The accumulation of the synthesized radiolabeled PanAm variants by saponin-isolated trophozoite-stage parasites was monitored over time and compared to accumulation of [^{14}C]Pan (Figure 3a). The PanAms were accumulated to higher concentrations inside the parasites than in the extracellular medium (i.e. distribution ratio > 1), consistent with the PanAms not just being taken up by the parasite, but also metabolised (Figure 3b and c). Importantly, no correlation was found between the accumulation profiles of N6-PanAm and *N*-Bn-PanAm and their antiplasmodial activities.

Interestingly, *N*-Bn-HoPanAm was accumulated to a much higher distribution ratio than its *n*-PanAm and α-PanAm counterparts and that of the N6-series; however, this increase does not correlate with it having improved antiplasmodial potency, as N6-PanAm—which is accumulated to a much lower distribution ratio—still has a lower antiplasmodial IC_{50} value (0.55 ± 0.1 μM compared to 4.7 ± 0.1 μM for *N*-Bn-HoPanAm[5]). Nonetheless, Pan still accumulates to a distribution ratio ~2-fold higher than that of *N*-Bn-HoPanAm, indicating a strong preference for the transport and/or metabolism of Pan compared to the PanAms (Figure 3a). To investigate this selectivity further, we studied the effect of increasing Pan concentrations on the accumulation of the radiolabeled PanAms. The IC_{50} values determined from the obtained activity profiles (Figure 3d and e) indicated that Pan had the most potent effect on the accumulation of the two α-PanAms, whereas HoPanAm and *n*-PanAm accumulation were inhibited to a lesser extent (Table 1, right).

To ascertain whether the compounds are being transported by the H^+-dependent Pan transporter, the distribution ratio was monitored after 30 minutes in the absence and presence of phloretin, which is a known Pan transport inhibitor.[14] Addition of phloretin blocked the accumulation of radiolabeled α-PanAms, but surprisingly the accumulation of the *n*-PanAms and HoPanAms variants was apparently stimulated by it (Figure 3f). This suggests that the α-PanAms enter the parasite through the Pan transporter, but that the *n*-PanAms and HoPanAms use alternative means to gain entry. The stimulation of the accumulation of the latter two variants—which is statistically significant in the case of the N6 derivatives (Figure 3f, $p = 0.0024$ for N6-

PanAm; $p = 0.04$ for N6-HoPanAm)—is in agreement with previous published work that showed that phloretin stimulates the uptake of pantothenol, another pantothenate analogue that exhibits antiplasmodial activity and targets CoA metabolism/utilization.[18,35] The reason for this stimulatory effect is still unclear, however it might be due to alleviation of feedback regulation of PanK by CoA.

To establish if the PanAms are transported by an alternative process dependent on the H^+ gradient across the parasite plasma membrane, the experiments were repeated in the presence of the ionophore carbonyl cyanide *m*-chlorophenyl hydrazine (CCCP), which is known to cause rapid dissipation of the H^+ gradient.[14] A similar trend was observed with accumulation of the α-PanAms being blocked by the ionophore, while the *n*-PanAms and HoPanAms still accumulated in the parasite in amounts comparable to the controls with no ionophore present (Figure 3f). Taken together, the data are consistent with the *n*-PanAms and HoPanAms being transported by an alternative process that is not dependent on the H^+ gradient—perhaps diffusion through the membrane, as has been shown to be the case for pantetheine in certain bacteria[36] and pantothenol in the parasite.[18] In contrast, uptake of the α-PanAms seems to occur by means of the *Plasmodium* Pan transporter.[14]

These results are consistent with the difference in the antiplasmodial activity of the three PanAm variants not being linked to the method of their uptake, but instead on a process related to Pan metabolism. This directed our attention to the first step of CoA biosynthesis, the phosphorylation of Pan to 4'-phosphopantothenate as mediated by *Pf*PanK (Figure 1a).

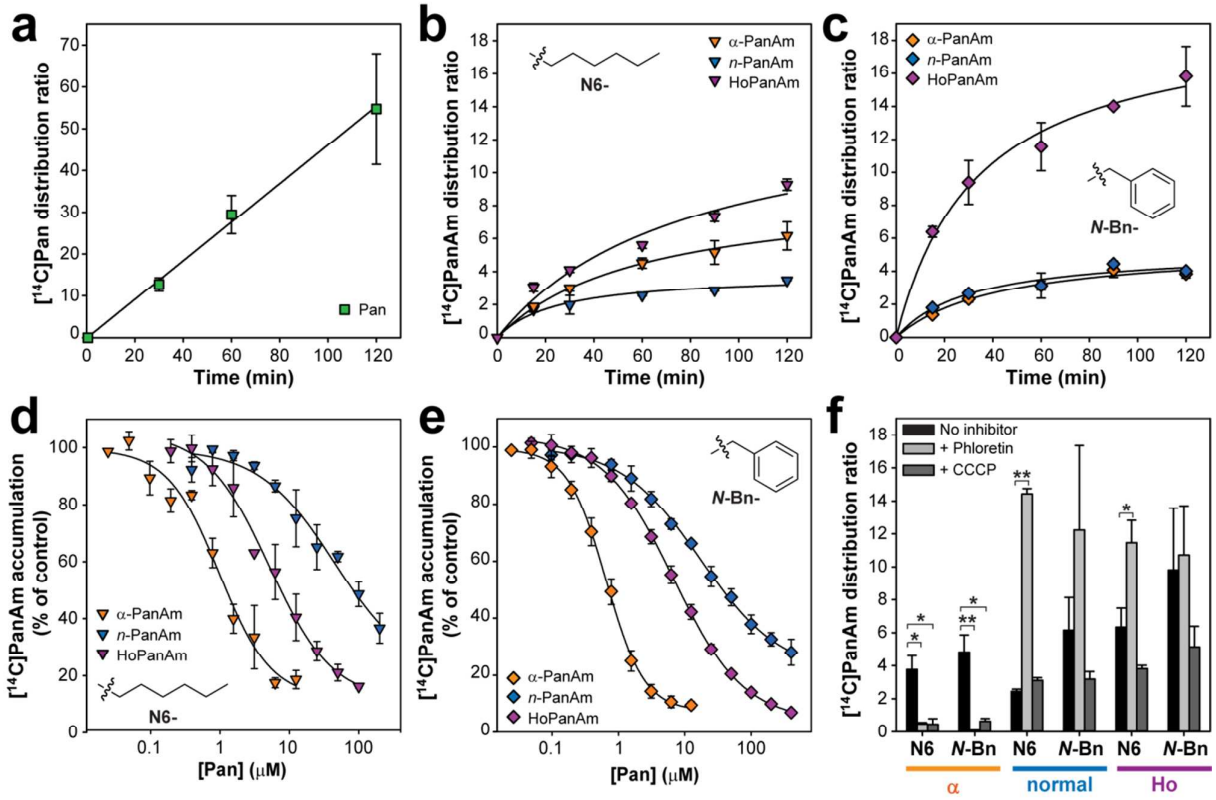

Figure 3. Accumulation of [^{14}C]Pan and [^{14}C]PanAm in saponin-isolated *P. falciparum* trophozoites. **a)** Accumulation of [^{14}C]Pan over 2 hours. Data represent an average of three separate experiments, each performed in duplicate and error bars denote SEM. **b)** Accumulation of the ^{14}C-labelled N6-series of PanAm variants over 2 hours. **c)** As for **b**, but for the ^{14}C-labelled *N*-Bn-series of PanAm variants. The data in panels **b** and **c** represent an average of two separate experiments, each performed in duplicate and error bars denote range/2. **d)** and **e)** Effect of increasing Pan concentration on [^{14}C]PanAm accumulation (panel **d** and **e** for the N6 and *N*-Bn series respectively) by saponin-isolated *P. falciparum* trophozoites after 60 minutes. Accumulation is plotted as percentage of a control with no Pan present. Both **d** and **e** represent an average of two separate experiments, each performed in duplicate and error bars denote range/2. **f)** Distribution ratio of both series of [^{14}C]PanAm variants after accumulation in isolated *P. falciparum* parasites for 30 minutes (indicated in black bars). Accumulation was also measured in the presence of 400 μM phloretin (light grey bars) and 10 μM CCCP (dark grey bars) for each compound under investigation. The data are an average of 2-4 separate experiments, each performed in duplicate and error bars denote SEM or range/2. Statistical analysis was done by performing an unpaired student's t-test (where * is $p < 0.05$ and ** is $p < 0.01$).

PanAm inhibition of Pan phosphorylation by *Pf*PanK in parasite lysates confirms an effect on metabolism, not uptake. The ability of the PanAms to interfere with the phosphorylation of [^{14}C]Pan by *Pf*PanK (either by direct inhibition or by acting as alternative substrates that compete with Pan for the enzyme's active site) was investigated using lysates prepared from isolated parasites. For these tests, unlabeled versions of the same PanAms (i.e. the N5 and *N*-PE-substituted series) that were used in the accumulation studies were investigated. *Pf*PanK activity was determined by measuring the amount of [^{14}C]Pan phosphorylated after 30 minutes (a time period during which Pan phosphorylation increased linearly under control conditions) in the presence or absence of the PanAm of interest. Concentration response profiles generated for each compound allowed the determination of IC_{50} values for the inhibition of [^{14}C]Pan phosphorylation (Figure 4a and b; Table 2). The results showed that for both sets of PanAms, the HoPanAm and *n*-PanAm variants were much more potent inhibitors of Pan phosphorylation than their α-PanAm counterparts, exhibiting IC_{50} values in the sub-micromolar range (0.2–0.4 μM) compared to values in the 7–9 μM range for the latter. These trends correlate directly with those observed for the inhibition of Pan accumulation (Figure 2a and 2b; Table 1, left), providing further evidence that the PanAms interfere with Pan metabolism, rather than its transport.

Table 2. Inhibition of *Pf*PanK-catalyzed phosphorylation of radiolabeled Pan by non-labeled PanAms.

Inhibition of phosphorylation of [^{14}C]Pan by indicated PanAm		
Non-labeled variant	IC_{50} (μM)[a]	
	N5 series	*N*-PE series
α-PanAm	7.6 ± 0.1	9.8 ± 0.9
n-PanAm	0.21 ± 0.02	0.21 ± 0.01
HoPanAm	0.43 ± 0.03	0.31 ± 0.01
Deoxy-PanAm	>100	11 ± 2
4'-phospho-PanAm	ND[b]	1.3 ± 0.2

[a] The IC_{50} of PanAm-mediated inhibition of [^{14}C]Pan phosphorylation by parasite lysates after a 45–60 minute incubation at 37 ºC. The reported values represent the average of two independent experiments, each performed in duplicate; the errors indicate the range/2.

[b] ND, not determined.

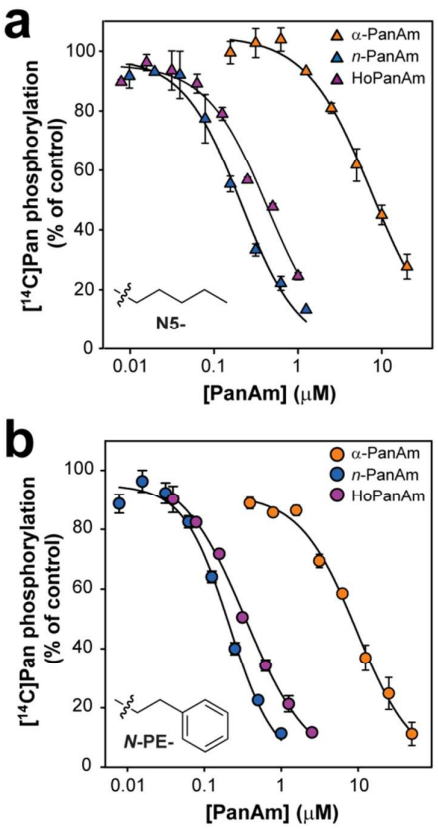

Figure 4. Inhibition of phosphorylation of 2 μM [^{14}C]Pan by *Pf*PanK present in parasite lysate by (**a**) N5- and (**b**) *N*-PE-substituted series of PanAm variants. Data were calculated as percentage of control reactions in which no PanAm was added (100% phosphorylation). For both panels **a** and **b** the data are an average of two separate experiments, each performed in duplicate; the error bars denote range/2.

***Pf*PanK phosphorylates the PanAms, showing kinetic distinction between the different variants and *N*-substituents.** Previous studies of the interaction of PanAms with *Sa*PanK showed similar results to those observed in the experiment described above: poor inhibition of Pan phosphorylation by the α-PanAm series, while members of both the *n*-PanAm and HoPanAm series potently inhibit Pan phosphorylation.[27] To establish if the observed inhibition of *Pf*PanK shows a similar distinction, we investigated whether the enzyme accepts PanAms as substrates using the synthesized radiolabeled N6-series, as well as [^{14}C]*N*-Bn-PanAm (insufficient amounts of the radiolabeled *N*-Bn-α-PanAm and *N*-Bn-HoPanAm variants were available to allow for their inclusion in these experiments).

Phosphorylation reactions performed with these compounds showed that they all act as substrates of *Pf*PanK, however, they are phosphorylated more slowly than Pan (Figure 5a). Activity profiles were next obtained for each compound from the initial rates measured over 30

minutes (the linear portion of the progress curves) using a range of concentrations (Figure 5b). From these profiles kinetic parameters were determined for each compound by fitting the data to either the Michaelis-Menten or Hill equation by non-linear regression (Table 3). The Hill equation was considered as a model for the kinetic data in light of the recent report of the allosteric behavior of the human PanK3 isoform (*Hs*PanK3).[37] Instead, we found that for *Pf*PanK the data for both Pan and N6-α-PanAm were still best described by the Michaelis-Menten equation. However, the Hill equation gave a better fit to the data obtained for N6-PanAm and HoPanAm, with Hill numbers greater than 1.5 in both cases, while the data for *N*-Bn-PanAm were described equally well by either equation. A Hill number >1.5 is consistent with *Pf*PanK positive cooperativity in certain cases, depending on the structure of the substrate and its interactions with the enzyme's active site (see below).

The determined kinetic parameters highlighted several trends (Table 3). Specifically, N6-HoPanAm showed $K_{0.5}$ and V_{max} values similar to the K_M and V_{max} obtained for Pan, while the parameters determined for N6-α-PanAm are much higher (K_M and V_{max} are ~13- and ~2.7-fold higher than the corresponding parameters for Pan, respectively). For the two *n*-PanAms the analysis is more complex. Both N6-PanAm and *N*-Bn-PanAm have $K_{0.5}$ values that are an order of magnitude lower than the K_M for Pan, indicating high affinity interactions with the enzyme. Moreover, their V_{max} values are also smaller than that of Pan, although the reduction is much larger in magnitude for *N*-Bn-PanAm than for its N6 counterpart.

Table 3. Kinetic parameters determined for the phosphorylation of Pan and PanAm variants by *Pf*PanK present in *P. falciparum* lysate.[a]

Radiolabeled substrate	K_M *or* $K_{0.5}$ (μM)	V_{max} (μmol.h^{-1} per 10^{12} parasites)	Hill number	Equation fitted
Pan	0.397 ± 0.092	13.2 ± 1.8	-	Michaelis-Menten
N6-α-PanAm	5.14 ± 1.97	36.7 ± 1.7	-	Michaelis-Menten
N6-PanAm	0.054 ± 0.012	8.58 ± 1.35	2.11 ± 0.01	Hill
N6-HoPanAm	0.180 ± 0.004	11.3 ± 2.2	1.57 ± 0.17	Hill
N-Bn-PanAm	0.013 ± 0.003	2.24 ± 0.11	1.17 ± 0.59	Hill

[a] The reported values represent the average parameters determined from of two independent experiments, each done in duplicate; the errors indicate the range/2.

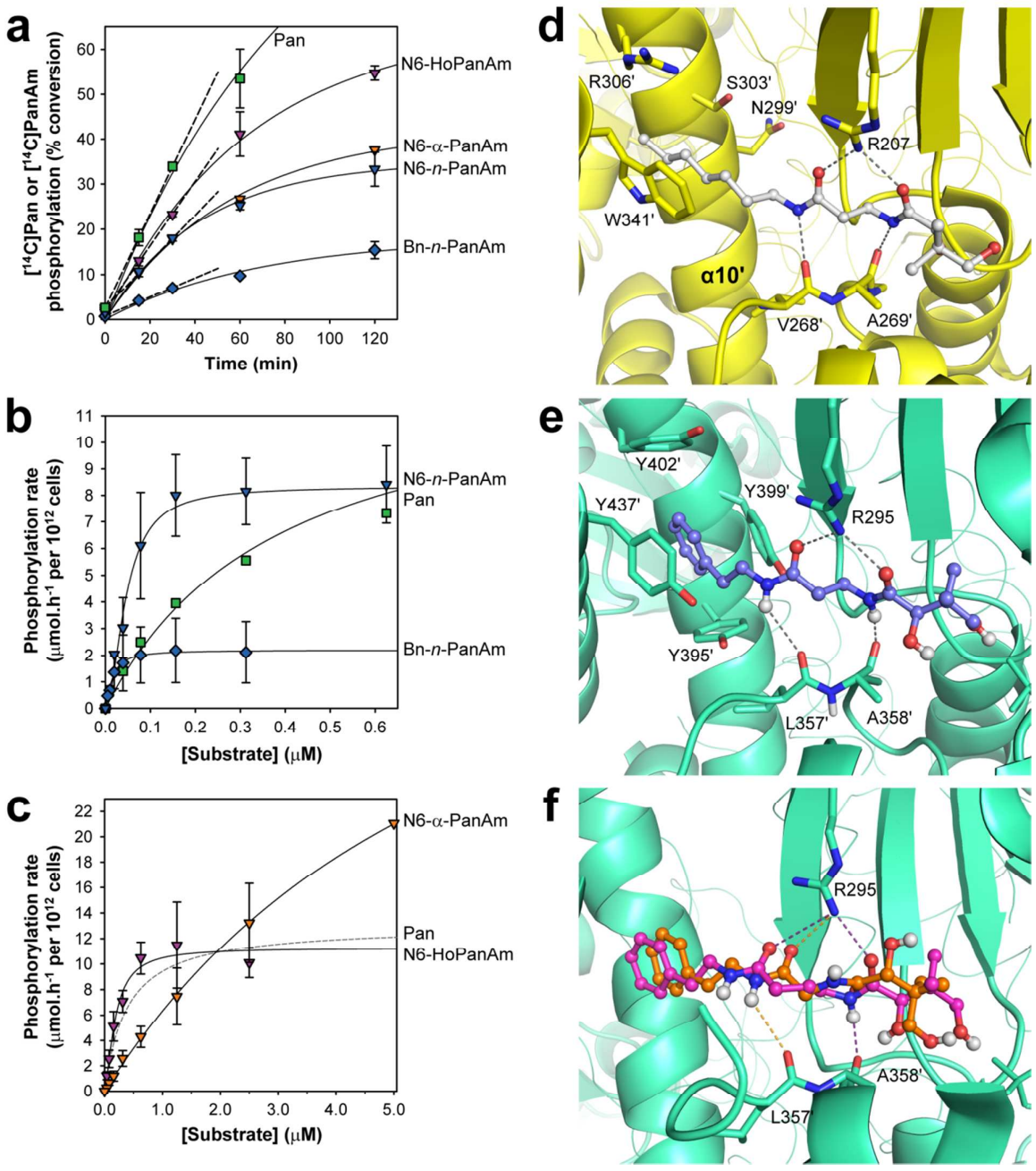

Figure 5. **a)** [^{14}C]PanAm phosphorylation by parasite lysate over 2 hours, shown as % conversion of total substrate added. Dashed lines indicate the linear portion of each curve, which is maintained over at least 30 min. The data are from one experiment performed in duplicate and error bars denote SD. **b)** Activity profiles of *Pf*PanK present in parasite lysate acting on [^{14}C]Pan, [^{14}C]N6- and [^{14}C]*N*-Bn-PanAm as substrates. **c)** Activity profiles of *Pf*PanK present in parasite lysate when supplied with increasing concentrations of [^{14}C]N6-α-PanAm or [^{14}C]N6-HoPanAm as substrates. The dashed line shows the Pan activity profile for reference. For both panels **b** and **c** the solid lines are the curves obtained from fitting either the Michaelis-Menten (for Pan and N6-α-PanAm) or Hill (for the *n*-PanAms and N6-HoPanAm) equations to the data. The data are an average of two separate experiments, each performed in duplicate and error bars denote range/2. **d)** Structure of *Hs*PanK3 with N7-Pan (stick structure with C-atoms in

white) bound in the active site (PDB id: 3SMS) showing the hydrogen bonding interactions with Arg207, which bridges the carbonyl oxygen atoms of the ligand's amide groups, as well as the hydrogen bonds between the backbone carbonyls of Val268' and Ala269' and the ligand's amide hydrogens. The four residues (N299', S303', R306' and W341') that are substituted for Tyr in *Pf*PanK are also indicated. **e)** Model of *Pf*PanK with *N*-PE-PanAm (stick structure with C-atoms in blue) bound showing the same hydrogen bonding interactions between the ligand and Arg295, Leu357' and Ala358'. The four Tyr residues (Tyr395', Tyr399', Tyr402' and Tyr437') that form the hydrophobic pocket that accommodates the phenyl group of the ligand are indicated. **f)** The same model of *Pf*PanK showing the α-PanAm (stick structure with C-atoms in orange) and HoPanAm (stick structure with C-atoms in magenta) variants of *N*-PE-PanAm bound. In the case of *N*-PE-HoPanAm, only the interactions between Arg295 and the ligand's proximal amide group, and between the same amide N–H and the backbone carbonyl of Ala358' are maintained (indicated with magenta dashes), while the distance between Arg295 and its distal amide increases, leading to a weakened or lost interaction. In contrast, *N*-PE-α-PanAm maintains interactions (shown in orange dashes) between its distal amide and Arg295 and Leu357' respectively, as the proximal amide is rotated away. The rotation also leads to a very different placement of the geminal dimethyl groups as well as the 4'-OH group that is to be phosphorylated. The amide substituent is still accommodated in the pocket formed by the Tyr residues shown in panel **e**, but these were omitted for clarity.

From this data set—the first to be obtained for *Pf*PanK with PanAms as substrates—we conclude that the core moiety of the PanAm dictates the affinity of the interaction of the substrate with *Pf*PanK, with the β-alanine moiety being preferred, while the amide substituent apparently affects the rate of turnover, at least in the *n*-PanAm series. Importantly, the data show that *Pf*PanK kinetically differentiates between the three PanAm variants in a manner similar to that described for *Sa*PanK above. However, the data obtained here show that the reduction in the V_{max} values for *Pf*PanK is not as extensive as was found for *Sa*PanK. Moreover, the difference in the V_{max} values determined for N6-PanAm and *N*-Bn-PanAm does not correlate with their antiplasmodial activities, as would be expected if reduced *Pf*PanK turnover was a factor in the PanAm's antiplasmodial MoA. Since the cost and difficulty in synthesizing an extended set of radiolabeled PanAms made an expanded structure activity relationship (SAR) analysis difficult, we decided to turn to the use of other tools to further investigate the interactions of the PanAms with *Pf*PanK.

The modeled *Pf*PanK active site interactions with the PanAms support the analysis drawn from the kinetic data. We first set out to investigate if we could gain information from the architecture of the *Pf*PanK active site. While the molecular identity of the *Pf*PanK is still to be

confirmed, and as a consequence there is no available crystal structure to investigate the interactions of the PanAms in the active site of the enzyme, the most likely *Pf*PanK candidate does show a high level of sequence similarity (apart from some parasite specific insertions) with the human PanK isoforms PanK1α and PanK1β, PanK2 and PanK3.[15] Among these, the co-crystal structure of the homodimeric *Hs*PanK3 with *N*-heptyl-*n*-pantothenamide (N7-Pan) and ADP bound in both active sites has been determined (PDB id: 3SMS). This structure shows that key substrate-recognizing interactions are the two hydrogen bonds made between the side chain of Arg207 and the two amide carbonyls of the PanAm, and the hydrogen bonds between the PanAm's amide N–H groups and the backbone carbonyls of Val268' and Ala269' (in the adjacent monomer) (Figure 5d). Since these hydrogen bonds frame the substrate's β-alanine moiety, we considered that these interactions could also be responsible for *Pf*PanK's selectivity for the PanAm variants. To investigate if this is indeed the case, the *Hs*PanK3 co-structure was used as a template to construct a model structure of *Pf*PanK (in which its parasite-specific inserts[15] are excluded) that could be used to interrogate its active site interactions. The structure of N7-Pan was modified *in situ* to reflect the structures of *N*-PE-PanAm (the most potent antiplasmodial *n*-PanAm discovered to date) and its α-PanAm and HoPanAm counterparts. All structures were subsequently re-docked into the active site of the *Pf*PanK model; to investigate the binding interactions between the enzyme and the PanAms further, molecular dynamics simulations were performed to compare the extent to which the observed binding interactions are maintained.

Based on the resulting model structures, we predict that *Pf*PanK forms the same key hydrogen bonding interactions with the two amide groups flanking the β-alanine moiety of *N*-PE-PanAm (Figure 5e). In addition, the molecular dynamics simulations indicated that these interactions are maintained in both active sites for the course of the 1.2 ns simulation. In the case of *N*-PE-HoPanAm introduction of the extra methylene group results in greater flexibility and loss of the hydrogen bond with the Leu357' backbone carbonyl, while the distance between its distal amide and Arg295 increases, leading to a potentially weaker interaction (Figure 5f). Simulation with *N*-PE-α-PanAm indicated the formation of alternate interactions with its amide groups (Figure 5f). The shortening of the distance between the amides due to the exchange of β-alanine for glycine apparently prevents both amide bonds from simultaneously forming the expected hydrogen bonds, resulting in fewer interactions with *Pf*PanK compared to the other two substrates. These differences correlate with the differences in *Pf*PanK's kinetic parameters for the three PanAm variants, and provide an explanation for the enzyme's preference for substrates in which the β-alanine moiety is maintained.

In addition to the hydrogen bonding interactions that are necessary for binding of the substrate, comparison of the *Pf*PanK model and the *Hs*PanK3 co-structure also revealed several

substitutions of polar residues for Tyr that result in the formation of a hydrophobic pocket in *Pf*PanK in the vicinity of the PanAm's amide substituent (Figure 5e). This hydrophobic pocket (a cage lined by Tyr395', Tyr399', Tyr402' and Tyr437') is likely to afford more favorable binding for PanAms substituted with alkyl, alkyl thioether and aromatic groups, compared to the natural substrate Pan. Furthermore, occupation of the hydrophobic pocket causes both amide bonds of the PanAms to lock into a favorable conformation for hydrogen bonding with the protein backbone, whereas the carboxylic acid group of Pan would remain free to rotate. Finally, the model with *N*-PE-PanAm bound highlights the formation of potential π-stacking interactions between the aromatic substituent and Tyr399' and Tyr437'. Such interactions would also explain the lower K_M determined for *N*-Bn-PanAm compared to N6-PanAm, as well as the former's lower V_{max} (due to slower release of its phosphorylated product). Overall, these observations correlate with *Pf*PanK having a preference for binding *n*-PanAms with hydrophobic, and specifically aromatic, substituents.

Poor inhibition of *Pf*PanK and *P. falciparum* by DL-4'-deoxy-PanAms point to *Pf*PanK not being the target of PanAm inhibition. The results of the modeling studies mirror the findings of the study on the interaction of antistaphylococcal PanAms with *Sa*PanK, which also showed preferential binding of *n*-PanAms with specific amide substituents.[27,38] Moreover, in the *Sa*PanK case a linear correlation was observed between an individual *n*-PanAm's IC_{50} value for inhibition of Pan phosphorylation and its k_{cat} value; subsequent experiments showed this to be due to the PanAms being trapped in the active site after being phosphorylated, strongly suggesting that inhibition of *Sa*PanK is an important contributor to the MoA of the PanAms in the inhibition of *S. aureus*.[33]

While it would be tempting to extrapolate the findings of the *S. aureus* study to *P. falciparum* and to conclude that the PanAms act against the parasite by inhibiting Pan phosphorylation, the observed trends in the antiplasmodial potency of the PanAm variants could also be explained by their selective metabolic activation (phosphorylation). Since the experimental limitations of performing extensive kinetic analysis of *Pf*PanK activity and inhibition in parasite lysates prevented us from performing a similar IC_{50}/V_{max} correlation analysis, we decided to turn to studying a different set of PanAm analogues to establish these compounds' antiplasmodial MoA. The *n*-PanAm analogues DL-4'-deoxy-N5-Pan (dN5-Pan) and DL-4'-deoxy-PE-PanAm (d*N*-PE-PanAm) were therefore prepared; these compounds have the same amide substitutions as N5-Pan and *N*-PE-PanAm respectively, but lack the 4'-hydroxyl group that is phosphorylated by PanK enzymes (Figure 6a).[27] While this exchange makes it impossible for the compound to be metabolically activated through phosphorylation, and

therefore to have any inhibitory effects on processes and enzymes other than *Pf*PanK, they are expected to maintain all the other important binding interactions with the enzyme. Consequently, one would expect such compounds to largely retain their antiplasmodial activity if inhibition of *Pf*PanK formed part of the MoA of the PanAms.

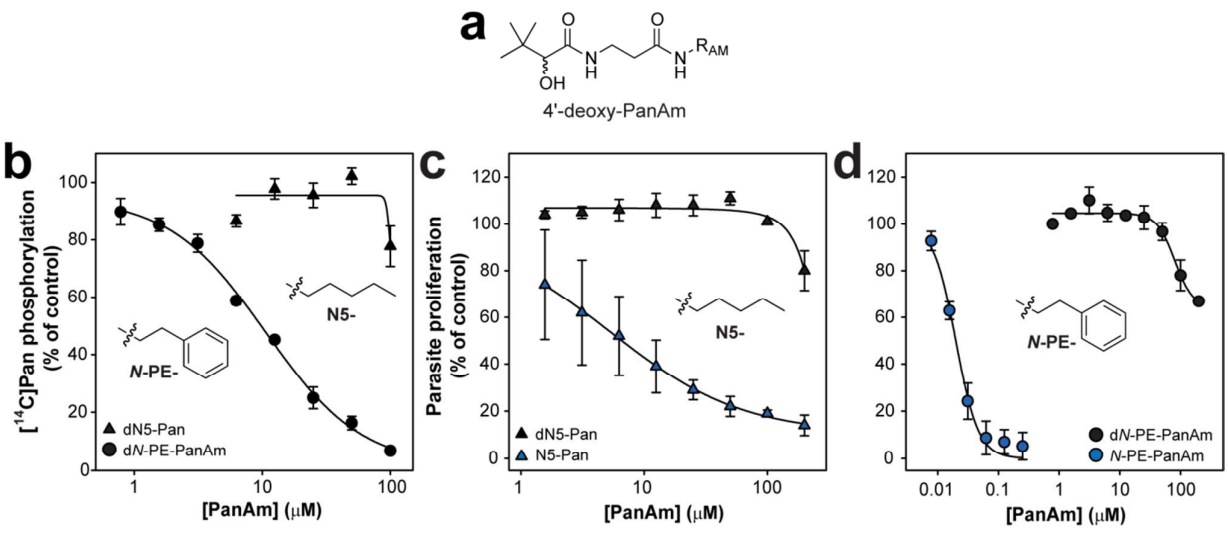

Figure 6. a) Chemical structure of DL-4'-deoxy-PanAms in which the 4'-OH-group of the parent compound is removed. **b)** Inhibition of phosphorylation of 2 μM [^{14}C]Pan by *Pf*PanK present in parasite lysate by dN5-Pan and d*N*-PE-PanAm. The data are an average of two separate experiments, each performed in duplicate; error bars denote range/2. **c)** and **d)** Antiplasmodial activity of N5-Pan (panel **c**) and *N*-PE-PanAm (panel **d**) in comparison to the corresponding deoxy variants of each compound in culture medium in which pantetheinase has been inactivated. Data for parent compounds are from previous published work.[4-5] Data for the deoxy-variants are an average of two separate experiments, each performed in triplicate and error bars denote range/2.

The interaction of dN5-Pan and d*N*-PE-PanAm with *Pf*PanK was first determined by measuring the phosphorylation of [^{14}C]Pan by parasite lysates in the presence of increasing concentrations of the two deoxy-compounds (Figure 6b). The IC_{50} values obtained from the resulting dose response profiles showed that d*N*-PE-PanAm has a ~500-fold reduction in inhibition potency compared to *N*-PE-PanAm, with an additional order of magnitude difference in the case of the N5 series compounds (Table 2). These results stand in contrast to those obtained for a similar experiment performed with *Sa*PanK and dN5-Pan and N5-Pan, which exhibited the same inhibitory effect on this enzyme.[27] The poor inhibition of *Pf*PanK-mediated Pan

phosphorylation by the DL-4'-deoxy-PanAms indicates that the 4'-OH group forms crucial binding interactions with the enzyme, and suggests that *Pf*PanK is predisposed to binding PanAms that can act as PanK substrates, i.e. compounds that can be metabolically activated through phosphorylation.

The poor interaction of dN5-Pan and d*N*-PE-PanAm with *Pf*PanK also suggested that these compounds would show poor antiplasmodial activity. Indeed, both DL-4'-deoxy-PanAms have antiplasmodial IC_{50} values >200 μM, while the two parent compounds showed potent antiplasmodial activities with IC_{50} values of 7.5 ± 6.2 μM and 0.020 ± 0.002 μM, respectively (Figure 6c and d).[4-5] Again, these findings do not correlate with results found in *S. aureus*, in which the dN5-Pan was only ~30-fold less potent than N5-Pan. Moreover, d*N*-PE-PanAm's ~10-fold higher inhibition of Pan phosphorylation compared to dN5-Pan did not translate to it showing a similarly higher parasite killing activity. Taken together, these results strongly indicate that the MoA of the PanAms is different in *S. aureus* and in *P. falciparum*, and that the inhibition of PanK does not play an important role in PanAm-mediated inhibition of proliferation of the latter.

4'-Phospho-*N*-PE-PanAm is a poor inhibitor of *Pf*PanK-mediated Pan phosphorylation, but still inhibits *P. falciparum* proliferation. The results obtained with the deoxy variants are consistent with the PanAms having to be metabolically activated through phosphorylation by *Pf*PanK to be able to exert an antiplasmodial effect. Consequently, phosphorylated PanAms can be expected to show antiplasmodial effects if they are stable under the growth assay conditions, and can cross the parasite membranes. Recently it was shown that 4'-phospho-pantetheine (P-PantSH), an intermediate in the CoA biosynthetic pathway and CoA degradation product that is structurally very similar to a phosphorylated PanAm, is stable in serum and can cross the membranes of several eukaryotic cell models.[39-40] We therefore prepared the phosphorylated version of *N*-PE-PanAm to determine if it has any effect on *Pf*PanK activity and on *P. falciparum* blood-stage proliferation.

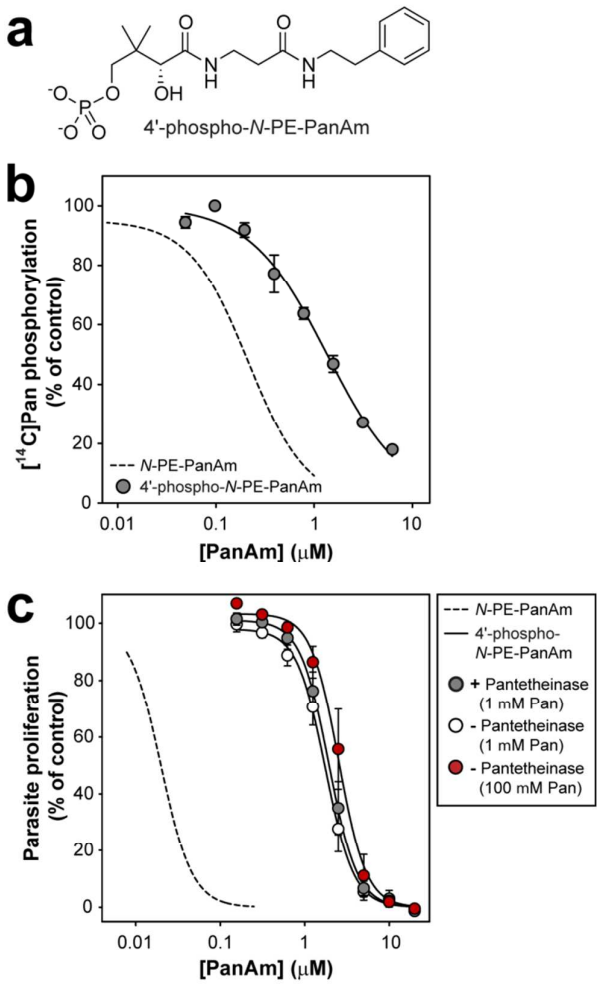

Figure 7. a) Chemical structure of 4'-phospho-*N*-PE-PanAm in which the 4'-OH-group of the parent compound is phosphorylated. **b)** 4'-Phospho-*N*-PE-PanAm-mediated inhibition of phosphorylation of 2 μM [^{14}C]Pan by *Pf*PanK present in parasite lysate. The data are an average of two separate experiments, each performed in duplicate and error bars denote range/2. The dotted line shows the fit for *N*-PE-PanAm-mediated inhibition (see Figure 4b) for comparison. **c)** Antiplasmodial activity of 4'-phospho-*N*-PE-PanAm in culture medium containing 1 μM Pan with and without pantetheinase activity. Activity was also measured in medium containing 100 μM Pan without pantetheinase activity. All data are an average of 3–4 separate experiments, each performed in triplicate; error bars denote SEM. The dotted line shows the fit for *N*-PE-PanAm-mediated inhibition (see Figure 6d) for comparison.

4'-Phospho-*N*-PE-PanAm (Figure 7a) was tested for its ability to inhibit the phosphorylation of [^{14}C]Pan by *Pf*PanK present in parasite lysate. While inhibition was observed, the determined IC_{50} of 1.3 ± 0.2 μM is 6.5 times higher than the value obtained for *N*-PE-PanAm (Figure 7b). This result provides evidence against a mechanism of inhibition similar to that seen for *Sa*PanK, where the phosphorylated PanAm is trapped in the enzyme.[33] However, 4'-phospho-*N*-PE-PanAm was found to still inhibit blood-stage parasite proliferation in culture media either

with or without pantetheinase, with IC_{50} values of 2.00 ± 0.25 μM and 1.84 ± 0.25 μM (SEM, n=4) respectively (Figure 7c). These values are relatively high compared to the value of ~20 nM determined previously for the parent compound (*N*-PE-PanAm) in media without pantetheinase[4]; this can likely be ascribed to the two compounds having different rates of uptake, although this remains to be tested. More importantly though, the observed antiplasmodial activity could not be antagonized by the addition of 100 μM Pan to the medium (IC_{50} 2.6 ± 0.5 μM; SEM, n=3) as could be done for the parent compound in a previous study,[4] indicating that the 4'-phospho version does not exert its antiplasmodial effect by inhibiting a process related to Pan accumulation (such as its phosphorylation by *Pf*PanK). Taken together, these results point to the PanAms exerting their antiplasmodial effects only after being metabolically activated into their phosphorylated forms by *Pf*PanK, and that *Pf*PanK itself is not the target of their inhibition. Consequently, the antagonism of the PanAm's antiplasmodial activity by increased amounts of Pan is best explained by the latter interfering with PanAm activation, and not through competition for the actual molecular target.

CONCLUSION

Although the antiplasmodial potential of the PanAms has been highlighted in several studies, little information was known regarding their MoA and the basis for the apparent requirement of the β-alanine moiety to retain activity against intraerythrocytic stage parasites. In this study, we demonstrated that differentiation between the PanAm variants is already established during uptake, with α-PanAms being transported by the H^+-mediated Pan transporter whereas *n*- and HoPanAm variants enter the parasite by a different route(s). However, we could find no evidence that inhibition of Pan uptake forms part of the PanAm's antiplasmodial MoA. Instead, our results show that upon uptake, *Pf*PanK phosphorylates the PanAms, and that the kinetic efficiency of this phosphorylation correlates with the antiplasmodial potency of the compounds. Since we found that *Pf*PanK prefers the PanAms as substrates over Pan, it is possible that PanAm treatment could initially lead to a temporary reduction in CoA levels as the PanAms outcompetes Pan for access to the enzyme. While such a process could be likened to the action of a competitive inhibitor acting on *Pf*PanK, the finding that the PanAms are also substrates of the enzyme means that the analysis of their inhibitory activity is more complex. In fact, our data indicate that *Pf*PanK's main role in the PanAms' MoA is to contribute to their metabolic activation through phosphorylation. Recently it was shown that the murine malaria parasites *Plasmodium yoelii* and *Plasmodium berghei* undergo normal asexual stage development even when lacking the genes encoding their putative PanK enzymes.[41-42] This could be explained by a

preference by these parasites to infect immature red blood cells (reticulocytes) that provide complex reservoirs of metabolites.

While we demonstrated that a phosphorylated PanAm has antiplasmodial activity, it is unclear whether it directly acts on a specific target, or is further activated by PPAT and DPCK into a CoA antimetabolite that act on CoA-dependent processes. The CoA biosynthetic enzymes PPCS and PPAT are both excellent candidates to act as the molecular targets of 4'-phospho-PanAms, especially since the former has been identified as the target of other phosphorylated Pan analogues (the fungal natural product CJ-15,801, and pantothenol) that show both antibacterial and antiplasmodial activity.[35,43-45] Whether it is a CoA-dependent process or a CoA biosynthetic enzyme, identification of the molecular target(s) of the activated PanAms remains an important goal considering that the citric acid cycle and fatty acid biosynthesis—both processes in which CoA plays a central role, and which otherwise would be considered to contain ideal target candidates—are not essential for survival of the blood-stage parasite.[46-48] Achieving this goal will therefore not only advance our search for new antiplasmodial agents, but will also make a significant contribution to our understanding of *P. falciparum* biology and its vulnerability related to its essential requirement for Pan.

METHODS

General materials and methods. Non-radiolabeled *N*-substituted PanAms and precursors previously published were prepared as previously described and their purity confirmed by ^{1}H, ^{13}C NMR and HRMS analysis.[2,5,27,34] The PanAms were dissolved in dimethylsulfoxide (DMSO) to yield stock solutions at a concentration of 200 mM and in all assays the final DMSO concentrations never exceeded 0.1% (v/v). General chemicals, reagents and media were purchased from Sigma-Aldrich (Aldrich, Sigma or Fluka), Merck Chemicals or BDH and were of the highest purity available. All solvents used were CHROMASOLV HPLC grade. Gentamycin and Albumax II for cell culture were obtained from Invitrogen. Scintillation fluid (MicroScint-O and MicroScint40), Whatman UNIFILTER 350 white opaque 96-well plates, and TopSeal-A Press-on Adhesive Sealing Film were purchased from Perkin-Elmer.

Analyses of all concentration-response curve data and Michaelis-Menten curves were done using Sigmaplot 12 (Systat software). For concentration-response curve data the percentage was plotted against the logarithm of increasing compound concentration and curve fitting was done by nonlinear regression (using the equation $y = a/(1 + (x/x_0)^b)$ to yield the compound concentration required for 50% inhibition of the process evaluated.

Synthesis of radiolabeled PanAms. Sodium D-[1-^{14}C]pantothenate ([^{14}C]pantothenate) with specific activity of 50 mCi/mmol was purchased from American Radiolabeled Chemicals, Inc. (S. Louis, Mo, USA) and was used in initial experiments. Radiolabeled versions of the N6- and *N*-Bn-series of PanAms were synthesized by modification of a method previously used to prepare non-radiolabeled PanAms,[34] using [1-^{14}C]*N*-hexylamine hydrochloride (55 mCi/mmol) and [7-^{14}C]*N*-benzylamine hydrochloride (55 mCi/mmol) (both obtained from American Radiolabeled Chemicals) as radioactive starting materials. Briefly, a 250 μL reaction mixture was constituted by combining the phenyl thioester of α-pantothenic acid, Pan, or homopantothenic acid (75 μL of a 20 mM solution in acetonitrile; 1.5 μmol), triethylamine (50 μL of a 20 mM solution in water; 1 μmol), the radiolabeled amine hydrochloride (50 μL of a 18.2 mM solution in water; 0.91 μmol; 50 μCi) and 75 μL acetonitrile. The mixture was incubated at 40 °C for 4 hours, followed by the addition of 1,4-diaminobutane (75 μL of a 20 mM solution in acetonitrile; 1.5 μmol) and incubation at 40 °C for a further hour. The mixture was then loaded onto a column of Amberlite IRC-86 ion-exchange resin (150 mg resin prewashed with 40% acetonitrile in water), and the column was washed with a solution of 40% acetonitrile in water (350 μL × 3). The combined eluates were evaporated to dryness in a speedvac. The residues were resuspended in 240 μL of a solution of 20% acetonitrile in water, and their radioactive purity confirmed by thin layer chromatography (TLC) analysis. Up to six such reaction mixtures were combined for preparative scale synthesis. If needed, samples were purified using silica solid phase extraction columns (1 g/6 mL Strata Si-1 SPE columns from Phenomenex) pre-equilibrated with a solution of 10% methanol in dichloromethane (DCM), and eluting with the same solution. Fractions containing radioactivity were pooled, evaporated and treated as above. Purity was estimated to be 85–95%, but yields were generally found not to exceed 30%. Final stocks of 0.1 μCi/mL were prepared in a solution of 10% acetonitrile in water and stored at -20 °C until needed.

Synthesis of PanAms. *DL-4'-Deoxy-N-pentyl pantothenamide (dN5-Pan).* dN5-Pan was synthesized as previously described.[27]

DL-4'-Deoxy-N-phenethyl pantothenamide (dN-PE-PanAm). d*N*-PE-PanAm was synthesized by modification of the method used to prepare dN5-Pan. To a solution of 3,3-dimethyl-2-oxo-*N*-(3-oxo-3-(phenethylamino)propyl)pentanamide (150 mg, 0.493 mmol) in anhydrous methanol (MeOH) (10 mL) at 0 °C under an inert atmosphere was added sodium borohydride (28.0 mg, 0.739 mmol) in small portions. The reaction mixture was stirred for 1 hour at 0 °C, and left to stir overnight at room temperature (RT). The reaction was quenched at 0 °C by the addition of sat. aqueous NH_4Cl (10 mL) and the MeOH was removed *in vacuo*. The aqueous solution was extracted with ethyl acetate (EtOAc) (3 × 15 mL) and the combined organic extracts

were dried (Na_2SO_4), filtered and concentrated *in vacuo* to yield the target compound (143 mg, 94 %) as a white solid. R_f = 0.35 (10% MeOH in DCM). δ_H (600 MHz; $CDCl_3$; 25°C) 0.98 (9H, s, -$(CH_3)_3$), 2.36 (2H, t, *J* = 6.0 Hz, -CH_2-), 2.80 (2H, t, *J* = 6.9 Hz, -CH_2-), 3.50-3.60 (4H, m, -$(CH_2)_2$-), 3.64 (1H, d, *J* = 5.3 Hz, -CH-), 5.63 (1H, br s, -NH-), 6.80 (1H, br s, -NH-), 7.18-7.25 (3H, m, arom) and 7.30-7.36 (2H, m, arom). O<u>H</u> proton not observed. δ_C (150 MHz; $CDCl_3$; 25°C) 28.6, 37.6, 37.8, 38.2, 38.2, 43.3, 82.1, 129.2, 131.2, 131.3, 141.2, 173.9 and 175.5. (HRMS) $[M+H]^+$ 307.2023 (Calculated $[C_{17}H_{27}N_2O_3]^+$ = 307.2022).

3,3-Dimethyl-2-oxo-N-(3-oxo-3-(phenethylamino)propyl)pentanamide. To a solution of 3-amino-*N*-phenethylpropanamide (480 mg, 2.50 mmol) in DCM (20 mL) at 0 °C was added *N*,*N*-diisopropylethylamine (449 µL, 2.58 mmol) drop-wise over 5 minutes under an inert atmosphere. 1-Hydroxybenzotriazole hydrate (59.3 mg, 0.439 mmol), 3,3-dimethyl-2-oxo-butyric acid[27] (358 mg, 2.75 mmol) and *N*-(3-dimethylaminopropyl)-*N*'-ethylcarbodiimide hydrochloride (480 mg, 2.50 mmol) were then added consecutively and the reaction mixture was stirred overnight at RT. The reaction was quenched by the addition of 3 M aqueous HCl (25 mL) and the organic layer was washed with 3 M aqueous HCl (1 × 25 mL) and sat. aqueous $NaHCO_3$ (1 × 25 mL). The organic layer was dried (Na_2SO_4), filtered and concentrated *in vacuo* before purification by flash column chromatography (FCC) (2:1 EtOAc: Hexanes) afforded the amide (150 mg, 20%) as a white powder. R_f = 0.35 (FCC conditions). δ_H (300 MHz; $CDCl_3$; 25°C) 1.32 (9H, s, -$(CH_3)_3$), 2.35 (2H, t, *J* = 6.0 Hz, -CH_2-), 2.79 (2H, t, *J* = 7.0 Hz, -CH_2-), 3.49-3.57 (4H, m, -$(CH_2)_2$-), 5.63 (1H, br s, -NH-), 7.15-7.26 (3H, m, arom), 7.28-7.33 (2H, m, arom) and 7.49 (1H, br s, -NH-). δ_C (100 MHz; $CDCl_3$; 25°C) 26.5, 35.3, 35.5, 35.8, 40.9, 43.1, 126.8, 128.8, 128.9, 138.9, 160.6, 171.0 and 203.3. (HRMS) $[M+H]^+$ 305.1874 (Calculated $[C_{17}H_{25}N_2O_3]^+$ = 305.1865).

3-Amino-N-phenethylpropanamide. To a solution of benzyl 3-oxo-3-(phenethylamino)propylcarbamate (950 mg, 2.91 mmol) in MeOH (50 mL) at RT was added 10% palladium on carbon (Pd/C) (124 mg, 1.16 mmol). The reaction atmosphere was filled with hydrogen (H_2) gas and the reaction mixture was stirred overnight at RT. The reaction mixture was filtered and concentrated *in vacuo* to give the amine (550 mg, 98%) as a white-yellow solid. R_f = product on baseline (10% MeOH in DCM). δ_H (600 MHz; $CDCl_3$; 25°C) 1.55 (2H, br s, -NH_2), 2.27 (2H, t, *J* = 6.0 Hz, -CH_2-), 2.80 (2H, t, *J* = 7.0 Hz, -CH_2-), 2.94 (2H, t, *J* = 6.0 Hz, -CH_2-), 3.49 (2H, q, *J* = 7.0 Hz, -CH_2-), 6.98 (1H, br s, -NH-), 7.19-7.24 (3H, m, arom) and 7.27-7.33 (2H, m, arom). δ_C (150 MHz; $CDCl_3$; 25°C) 38.3, 40.7, 41.0, 43.0, 129.0, 131.1, 131.4, 141.0 and 175.0. (HRMS) $[M+H]^+$ 193.1343 (Calculated $[C_{11}H_{17}N_2O]^+$ = 193.1341).

Benzyl 3-oxo-3-(phenethylamino)propylcarbamate. Phenethylamine (621 µL, 4.93 mmol) and diethyl cyanophosphonate (748 µL, 4.93 mmol) were added to a solution of Cbz-β-alanine (1.00 g, 4.48 mmol) in anhydrous dimethylformamide (7 mL) at RT under an inert atmosphere.

The reaction mixture was cooled to 0 °C before triethylamine (1.31 mL, 9.41 mmol) was added. The reaction mixture was stirred for 2 hours at 0 °C and left to stir overnight at RT. EtOAc (50 mL) was added and the organic layer was washed with 5% aqueous citric acid (3 × 10 mL), 1 M aqueous $NaHCO_3$ (2 × 10 mL) and sat. aqueous NaCl (1 × 10 mL). The organic layer was dried (Na_2SO_4), filtered and concentrated *in vacuo* to afford the carbamate (1.45 g, 99%) as a white solid. R_f = 0.30 (3:1 EtOAc: Hexanes). δ_H (300 MHz; $CDCl_3$; 25°C) 2.34 (2H, t, *J* = 5.9 Hz, -CH_2-), 2.78 (2H, t, *J* = 6.9 Hz, -CH_2-), 3.43 (2H, q, *J* = 6.2 Hz, -CH_2-), 3.48 (2H, q, *J* = 7.0 Hz, -CH_2-), 5.09 (2H, s, -CH_2-), 5.38 (1H, br s, -NH-), 5.52 (1H, br s, -NH-) and 7.16-7.36 (10H, m, arom). δ_C (75 MHz; $CDCl_3$; 25°C) 35.6, 36.0, 37.2, 40.6, 66.6, 126.6, 128.0, 128.5, 128.6, 136.6, 138.8, 156.6 and 171.3. (HRMS) $[M+H]^+$ 327.1705 (Calculated $[C_{19}H_{23}N_2O_3]^+$ = 327.1709).

4'-Phospho-N-phenethyl pantothenamide (4'-phospho-N-PE-PanAm). To a solution of *N*-phenethyl pantothenamide 4'-*O*,*O*-dibenzylphosphate (120 mg, 0.206 mmol) in MeOH (9 mL) and H_2O (1 mL) at RT was added 10% Pd/C (31.3 mg, 0.294 mmol). The reaction atmosphere was filled with H_2 gas and the reaction mixture was stirred overnight at RT. The reaction mixture was filtered and concentrated *in vacuo* to give the target compound (82.3 mg, 99%) as a clear oil. R_f = 0.06 (10% MeOH in DCM). δ_H (300 MHz; D_2O; 25°C) 0.76 (3H, s, -CH_3), 0.83 (3H, s, -CH_3), 2.26 (2H, t, *J* = 6.7 Hz, -CH_2-), 2.66 (2H, t, *J* = 6.7 Hz, -CH_2-), 3.25-3.37 (4H, m, -$(CH_2)_2$-), 3.48 (1H, dd, *J* = 5.0, 9.7 Hz, -CH_2-), 3.68 (1H, dd, *J* = 4.7, 10.0 Hz, -CH_2-), 3.87 (1H, s, -CH-), 7.14-7.18 (2H, m, arom) and 7.22-7.30 (3H, m, arom). O<u>H</u> protons not observed. δ_C (75 MHz; D_2O; 25°C) 19.2, 21.2, 35.1, 36.1, 38.9, 39.0, 41.2, 72.1, 75.0, 127.2, 129.3, 129.5, 139.8, 174.3 and 175.4. δ_P (161.9 MHz; D_2O; 25°C) 3.43. (HRMS) $[M+H]^+$ 403.1625 (Calculated $[C_{17}H_{28}N_2O_7P]^+$ = 403.1634).

N-Phenethyl pantothenamide 4'-O,O-dibenzylphosphate. Dibenzyl chlorophosphate was prepared *in situ* by reacting *N*-chlorosuccinimide (373 mg, 2.79 mmol) and dibenzylphosphite (732 mg, 2.79 mmol) in anhydrous toluene (4 mL) under an inert atmosphere for 2 hours at RT. The reaction mixture was filtered to remove the succinimide. To a solution of *N*-PE-PanAm[33] (300 mg, 0.931 mmol) in anhydrous pyridine (5 mL) at -40 °C under an inert atmosphere was added dibenzyl chlorophosphate drop-wise with stirring. The reaction mixture was stirred for an additional 2 hours at -40 °C and the mixture was placed in the -20 °C freezer overnight. The reaction mixture was allowed to warm to RT and was subsequently quenched with H_2O (3 mL) and concentrated *in vacuo*. The resulting crude residue was re-dissolved in EtOAc (40 mL) and the organic layer was washed with 1 M aqueous H_2SO_4 (2 × 10 mL), 1 M aqueous $NaHCO_3$ (2 × 10 mL) and sat. aqueous Na_2SO_4 (1 × 10 mL). The organic layer was dried (Na_2SO_4), filtered and concentrated *in vacuo* before purification by FCC (5% MeOH in DCM) afforded the compound (150 mg, 28%) as a yellow oil. R_f = 0.11 (FCC conditions). δ_H (600 MHz; $CDCl_3$; 25°C) 0.80

(3H, s, -CH_3), 1.04 (3H, s, -CH_3), 2.34 (2H, t, J = 4.3 Hz, -CH_2-), 2.76 (2H, t, J = 7.2 Hz, -CH_2-), 3.44-3.52 (4H, m, -$(CH_2)_2$-), 3.55 (1H, dd, J = 7.6, 10.3 Hz, -CH_2-), 3.88 (1H, s, -CH-), 3.98 (1H, dd, J = 6.9, 9.5 Hz, -CH_2-), 5.03 (2H, d, J = 8.8 Hz, -CH_2-), 5.05 (2H, d, J = 8.2 Hz, -CH_2-), 6.16 (1H, br t, J = 5.6 Hz, -NH-), 7.02 (1H, br s, -NH-), 7.16-7.23 (5H, m, arom) and 7.28-7.38 (10H, m, arom). O<u>H</u> proton not observed. δ_C (150 MHz; $CDCl_3$; 25°C) 19.4, 21.9, 36.0, 36.3, 36.7, 40.1, 41.4, 70.4, 70.5, 74.2, 74.3, 120.9, 124.3, 127.2, 128.7, 129.3, 129.4, 136.0, 139.5, 171.8 and 173.2. δ_P (161.9 MHz; $CDCl_3$; 25°C) 0.79. (HRMS) $[M+H]^+$ 583.2575 (Calculated $[C_{31}H_{40}N_2O_7P]^+$ = 583.2573).

***P. falciparum* culture and growth assay.** All malaria parasite experiments were performed using the 3D7 strain of *P. falciparum* and were maintained in synchronous continuous cultures as described previously.[4-5] In general, growth assays were performed in media containing no pantetheinase activity, prepared as previously described.[2,4-5] However, the antiplasmodial activity of 4'-phospho-*N*-PE-PanAm was also determined in media with pantetheinase activity present as previously described.[5] Dose-response curves were determined with two-fold serial dilutions of 4'-deoxy-PanAms (from 0.391 μM to 200 μM) used in triplicate in a final volume of 200 μL. Experiments for the PanAms, N5-Pan (from 0.391 μM to 200 μM) and *N*-PE-PanAm (from 1.95 nM to 2 μM) were also included as controls for comparative reasons. The antiplasmodial activity of 4'-phospho-*N*-PE-PanAm was also evaluated by testing two-fold serial dilutions (from 0.156 to 20 μM) in triplicate in a final volume of 200 μL.

***P. falciparum* parasite isolation.** Mature trophozoite-stage parasites were isolated from the host erythrocytes as described previously.[16] Briefly, infected erythrocytes were treated with saponin (0.05% (w/v)) and centrifuged immediately for 8 minutes at 2,000 × *g* at RT. The supernatant was discarded and the resulting pellet washed by resuspension in malaria saline (25 mM HEPES (pH 7.1), 125 mM NaCl, 5 mM KCl, 20 mM glucose and 1 mM $MgCl_2$) followed by centrifugation at 14,000 × *g* for 30 seconds. The supernatant was discarded and the pellet washed an additional 3-4 times until the supernatant became clear. The isolated parasites were resuspended in malaria saline and either used immediately or incubated at 37 °C until used.

Accumulation of radiolabeled compounds in isolated parasites. Accumulation of radiolabeled compounds was measured essentially as described previously.[16] Briefly, isolated parasites were suspended in saline (25 mM HEPES (pH 7.1), 125 mM NaCl, 5 mM KCl, 20 mM glucose and 1 mM $MgCl_2$) at 37 °C; for experiments with transporter blockers, either 400 μM phloretin or 10

μM CCCP was included. Each reaction mixture contained a final concentration of 0.05 μCi/mL radiolabeled compound (equivalent to 1.0 μM [^{14}C]Pan or 0.9 μM [^{14}C]PanAms) and a final parasite concentration ranging between 5×10^7 to 1×10^8 parasites/mL. Reactions were initiated by the addition of the radiolabeled compound. At pre-determined time points 200 μL aliquots of the reactions were removed in duplicate and layered onto 200 μL of oil (5:4 mixture of dibutyl phthalate-dioctyl pthalate). Accumulation of the radiolabeled compounds was then immediately terminated by centrifugation at 15,800 × *g* for 2 minutes which facilitated sedimentation of the cells below the oil and thereby separated them from the aqueous solution containing the radiolabeled compound. The aqueous supernatant was aspirated and the tube rinsed 4 times with water. The oil was removed by aspiration and the cell pellet lysed with 0.1% (v/v) Triton X-100 (500 μL) and deproteinized by the addition of 5% (w/v) trichloroacetic acid (500 μL). After centrifugation at 10,000 × *g* for 10 minutes the supernatant was transferred to scintillation vials in preparation for scintillation counting.

For [^{14}C]Pan accumulation experiments the amount of radioactivity trapped in the extracellular portion of the cell pellet was estimated in a separate batch of cells treated with 400 μM phloretin in order to inhibit the Pan transporter.[14] The phloretin-treated cells were mixed with [^{14}C]Pan as described above. Aliquots were sampled immediately for centrifugation through the oil mix and subsequent processing. The counts per minute (CPM) in the pellets derived from phloretin-treated cells were subtracted from those obtained in untreated samples providing a measurement of the intracellular [^{14}C]Pan, from which distribution ratios could be determined. For [^{14}C]PanAm accumulation experiments the total initial amount of extracellular radioactivity was estimated by measuring the radioactivity in the supernatant of a "t=0" sample, i.e. a sample prepared by centrifugation through the oil mix immediately after mixing. An intracellular water volume of 28 fL for isolate *P. falciparum* parasites[16] was used to calculate distribution ratios.

To determine the accumulation of [^{14}C]Pan in the presence of non-radiolabeled PanAms, or [^{14}C]PanAms in the presence of non-radiolabeled Pan, experiments were performed as above, except that the solution of radiolabeled compound used to initiate the reaction also included increasing concentrations of the appropriate non-radiolabeled compound. Each reaction mixture contained a final concentration of either 0.1 μCi/mL [^{14}C]Pan (equivalent to 2.0 μM) or 0.08 μCi/mL of the appropriate [^{14}C]PanAm (equivalent to 1.45 μM), a final parasite concentration ranging between 3.2×10^7 to 7.2×10^7 parasites/mL, and varying concentrations of unlabeled substrate. Reactions were stopped after either 20 or 60 minutes (for accumulation of [^{14}C]Pan and [^{14}C]PanAms respectively), and the samples were processed exactly as described above. Dose-

response curves were determined relative to the total amount of labeled compound taken up by parasites incubated in the absence of unlabeled compound.

***P. falciparum* lysate preparation.** Parasite lysates were prepared from washed, saponin-isolated intact *P. falciparum* trophozoites as described before.[14] The parasites were lysed by suspension in cold 10 mM Tris (pH 7.4) and trituration (10×) through a 25-gauge needle. Particulate matter was removed from lysates in one of two ways: (i) lysates were centrifuged three times at 2,000 × *g* for 30 minutes at 4 °C; or (ii) lysates were centrifuged once at 17,000 × *g* for 30 minutes at 4 °C. Lysates were stored at -20 or -80 °C until required.

Time-course of phosphorylation of [^{14}C]Pan and [^{14}C]PanAms by *Pf*PanK. Parasite lysates were used to assess the ability of *Pf*PanK to phosphorylate radiolabeled Pan or PanAms over time. The phosphorylation experiments were performed using a modified version of the Somogyi reagent-based method.[19] Mixtures containing kinase buffer with a final composition of 50 mM Tris (pH 7.4), 5 mM ATP and 5 mM $MgCl_2$ and the radiolabeled compounds (0.1 μCi/mL, equivalent to 2.0 μM) to be tested were incubated for 10 minutes at 37 °C. The phosphorylation reaction was initiated by the addition of parasite lysate equivalent to 2.0–2.5 × 10^7 cells/mL. The reaction mixtures were incubated at 37 °C for 120 minutes, and at specific time points 50 μL of the reaction mixtures was transferred to wells of Whatman 96-well UNIFILTER 350 plates (containing 0.45 μm PP filter bottom and short drip directors) in duplicate. Each well was pre-loaded with 50 μL 150 mM $Ba(OH)_2$ and the reaction mixture was rapidly mixed with this solution by pipetting to terminate the phosphorylation reaction by protein precipitation. To each well 150 mM $ZnSO_4$ (50 μL) was added to allow precipitation of phosphorylated compounds. Non-phosphorylated compounds were removed by filtration under vacuum, leaving phosphorylated compounds trapped on the filters of each well. The filters were washed with water (2 × 200 μL), and subsequently 95% (v/v) ethanol (200 μL) and kept under vacuum for 30 minutes before being placed in an incubator to dry overnight at 37 °C. MicroScint-O (30 μL) was added to each well and immediately sealed (top and bottom) with TopSeal-A Press-on Adhesive Sealing Film. The radioactivity in each well was measured immediately by scintillation counting in a TopCount Microplate Scintillation and Luminescence Counter (Packard).

To determine total radioactivity so as to allow the conversion of radioactivity in CPM values into molar concentrations, two 50 μL aliquots of the reaction mixtures were mixed with 150 μL MicroScint-O in the wells of a 96-well OptiPlate. The plate was thereafter sealed with

TopSeal-A Press-on Adhesive Sealing Film and the radioactivity of each well measured by scintillation counting as described above.

Dose-response curves for the inhibition of *Pf*PanK-catalyzed [^{14}C]Pan phosphorylation by non-radiolabeled compounds were generated using the same procedure as for the time-course experiments. Phosphorylation was allowed to take place for 30–60 minutes (when a linear reaction rate applies under control conditions) before 50 µL aliquots were transferred to 96-well Whatman UNIFILTER 350 plates in duplicate. The plates were processed as described above to determine scintillation count. Control reactions containing 10 mM Tris (pH 7.4) served as blank reactions containing no parasite lysate, whereas reactions containing no PanAm served as positive controls that represented 100% phosphorylation.

Determining kinetic parameters for *Pf*PanK phosphorylation. Kinetic parameters were determined by performing phosphorylation reactions with each radiolabeled compound at concentrations that varied between 0.005 and 5.0 µM, depending on the substrate. Each compound was incubated at a specific concentration in kinase buffer and after addition of lysate allowed to be phosphorylated by *Pf*PanK for 30 minutes at 37 °C in a similar fashion as described above. Control reactions containing 10 mM Tris (pH 7.4) were used as blank reactions containing no parasite lysate. Kinetic parameters (V_{max} and either K_M and $K_{0.5}$, as appropriate) were determined by fitting either the Michaelis-Menten or Hill equations to the curves generated from the initial rated data obtained in this manner.

Modeling of PanAms into *Pf*PanK. The structure of *Pf*PanK was predicted by homology modeling, using the human PanK3 (PDB code: 3SMS) bound with N7-Pan and ADP as the template structure. The biological unit 3SMS was prepared on the PDB website (www.rscb.org) in order to model the homo-dimer. The sequence of *Pf*PanK and human PanK were aligned against the PFAM seed alignment for type II PanKs (PF03630) using T-COFFEE,[49] followed by manual adjustments to minimize gaps and insertions. Homology models of *Pf*Pank including ligands N7-Pan and ADP were built using MODELLER 9.13.[50] Considerable portions of *Pf*PanK do not align with cognate sequences. In order to keep the total atomic system a manageable size, the *N*-terminus (first 18 residues) and the loop from His37 to Asp61 were left unmodeled or deleted prior to subsequent modeling. The Schrödinger software suite (2015-1) was used for subsequent docking and molecular dynamics. N7-Pan was modified *in situ* to generate the *N*-PE-PanAm series. *N*-PE-PanAm (as well as the α- and homo counterparts) were subsequently re-docked into each active site using the GLIDE module.[51] High-scoring poses of each compound were chosen for both sites to prepare the system for molecular dynamics with DESMOND using

the OPLS2005 or OPLS2.1 forcefields.[52-53] *Pf*PanK models with ADP and the various *N*-PE-PanAm variants bound to both sites were hydrogenated and solvated in 10 Å buffer of TIP3 waters and 0.15 M NaCl, yielding a total system size of ± 65 000 atoms. Each system was relaxed using the default protocol and then simulated at 300 K and 1 bar for a total of 1.2 ns.

AUTHOR INFORMATION

Corresponding Authors

*(Marianne de Villiers) E-mail: mdevilliers@sun.ac.za

*(Erick Strauss) E-mail: estrauss@sun.ac.za

Author Contributions

M.deV.: Carried out accumulation, phosphorylation and parasite proliferation experiments, analyzed data and co-wrote the manuscript.

C.S.: Carried out accumulation, phosphorylation and parasite proliferation experiments, analyzed data and co-wrote the manuscript.

C.J.M.: Carried out phosphorylation and parasite proliferation experiments, and analyzed data.

L.B.: Synthesized PanAms.

G.W.: Performed modeling experiments.

K.J.S.: Conceptualized the project, co-directed the study, analyzed data and co-wrote the manuscript.

E.S.: Conceptualized the project, co-directed the study, synthesized radiolabeled PanAms, carried out accumulation experiments, analyzed data and co-wrote the manuscript.

All authors edited the manuscript.

Notes

The authors declare no competing financial interest.

ACKNOWLEDGMENTS

This project was funded by grants from the South African Malaria Initiative to E.S. and K.J.S. M.deV., C.J.M., L.B. and G.W. were supported by bursaries/fellowships from the National Research Foundation (NRF) of South Africa. C.S. was funded by an NHMRC Overseas Biomedical Fellowship (1016357). Support from the Oppenheimer Memorial Trust (to M.deV. and E.S.) and Australia Awards, an Initiative of the Australian Government (to C.J.M.), made visits to the ANU possible and are gratefully acknowledged. We are also grateful to the Canberra

Branch of the Australian Red Cross Blood Service (Australia) and the Western Cape Blood Bank (South Africa) for the provision of red blood cells.

ABBREVIATIONS

ACP, acyl carrier protein

ADP, adenosine diphosphate

ATP, adenosine triphosphate

CCCP, carbonyl cyanide *m*-chlorophenyl hydrazine

CPM, counts per minute

DCM, dichloromethane

DMSO, dimethylsulfoxide

dN5-Pan, 4'-deoxy-*N*-pentyl pantothenamide

d*N*-PE-PanAm, 4'-deoxy-*N*-phenethyl pantothenamide

dPCoA, 3'-dephospho-coenzyme A

DPCK, dephospho-CoA kinase

EtOAc, ethyl acetate

HEPES, 4-(2-hydroxyethyl)-1-piperazineethanesulfonic acid

HoPanAm, homopantothenamide

*Hs*PanK3, *Homo sapiens* pantothenate kinase 3

IC_{50}, concentration that gives half-maximal inhibition

MeOH, methanol

MoA, mode of action

α-PanAm, α-pantothenamide

N5-Pan, *N*-pentyl pantothenamide

N6-α-PanAm, *N*-hexyl α-pantothenamide

N6-HoPanAm, *N*-hexyl homopantothenamide

N6-PanAm, *N*-hexyl pantothenamide

N7-Pan, *N*-heptyl pantothenamide

N-Bn-α-PanAm, *N*-benzyl α-pantothenamide

N-Bn-HoPanAm, *N*-benzyl homopantothenamide

N-Bn-PanAm, *N*-benzyl pantothenamide

N-PE-α-PanAm, *N*-phenethyl α-pantothenamide

N-PE-HoPanAm, *N*-phenethyl homopantothenamide

N-PE-PanAm, *N*-phenethyl pantothenamide

P-Pan, 4'-phosphopantothenic acid

P-PanCys, 4'-phosphopantothenoylcysteine

P-PantSH, 4'-phosphopantetheine

Pan, pantothenate

PanAm, pantothenamide

PanK, pantothenate kinase

PantSH, pantetheine

*Pf*PanK, *Plasmodium falciparum* pantothenate kinase

4'-Phospho-*N*-PE-PanAm, 4'-phospho-*N*-phenethyl pantothenamide

PPAT, phosphopantetheine adenylyltransferase

PPCDC, phosphopantothenoylcysteine decarboxylase

PPCS, phosphopantothenoylcysteine synthetase

RT, room temperature

*Sa*PanK, *Staphylococcus aureus* pantothenate kinase

SEM, standard error of the mean

TLC, thin layer chromatography

REFERENCES

1. Pett, H. E., Jansen, P. A., Hermkens, P. H., Botman, P. N., Beuckens-Schortinghuis, C. A., Blaauw, R. H., Graumans, W., van de Vegte-Bolmer, M., Koolen, K. M., Rutjes, F. P., Dechering, K. J., Sauerwein, R. W., and Schalkwijk, J. (2015) Novel pantothenate derivatives for anti-malarial chemotherapy. *Malar. J. 14*, 169. DOI: 10.1186/s12936-015-0673-8
2. Macuamule, C. J., Tjhin, E. T., Jana, C. E., Barnard, L., Koekemoer, L., de Villiers, M., Saliba, K. J., and Strauss, E. (2015) A pantetheinase-resistant pantothenamide with potent, on-target, and selective antiplasmodial activity. *Antimicrob. Agents Chemother. 59*, 3666-8. DOI: 10.1128/AAC.04970-14
3. Hoegl, A., Darabi, H., Tran, E., Awuah, E., Kerdo, E. S., Habib, E., Saliba, K. J., and Auclair, K. (2014) Stereochemical modification of geminal dialkyl substituents on pantothenamides alters antimicrobial activity. *Bioorg. Med. Chem. Lett. 24*, 3274-7. DOI: 10.1016/j.bmcl.2014.06.013
4. Spry, C., Macuamule, C., Lin, Z., Virga, K. G., Lee, R. E., Strauss, E., and Saliba, K. J. (2013) Pantothenamides are potent, on-target inhibitors of *Plasmodium falciparum* growth when serum pantetheinase is inactivated. *PLoS One 8*, e54974. DOI: 10.1371/journal.pone.0054974
5. De Villiers, M., Macuamule, C., Spry, C., Hyun, Y.-M., Strauss, E., and Saliba, K. J. (2013) Structural modification of pantothenamides counteracts degradation by pantetheinase and improves antiplasmodial activity. *ACS Med. Chem. Lett. 4*, 784-789. DOI: 10.1021/ml400180d
6. *World Malaria Report 2015*; 2015.
7. Kaskow, B. J., Michael Proffit, J., Blangero, J., Moses, E. K., and Abraham, L. J. (2012) Diverse biological activities of the vascular non-inflammatory molecules – The Vanin pantetheinases. *Biochem. Biophys. Res. Commun. 417*, 653-658. DOI: 10.1016/j.bbrc.2011.11.099

8. Pace, H., and Brenner, C. (2001) The nitrilase superfamily: classification, structure and function. *Genome Biol. 2*, reviews0001.1-reviews0001.9
9. Jansen, P. A. M., Hermkens, P. H. H., Zeeuwen, P. L. J. M., Botman, P. N. M., Blaauw, R. H., Burghout, P., van Galen, P. M., Mouton, J. W., Rutjes, F. P. J. T., and Schalkwijk, J. (2013) Combination of Pantothenamides with Vanin Inhibitors as a Novel Antibiotic Strategy against Gram-Positive Bacteria. *Antimicrob. Agents Chemother. 57*, 4794-4800. DOI: 10.1128/aac.00603-13
10. Saliba, K. J., and Spry, C. (2014) Exploiting the coenzyme A biosynthesis pathway for the identification of new antimalarial agents: the case for pantothenamides. *Biochem. Soc. Trans. 42*, 1087-93. DOI: 10.1042/BST20140158
11. Moolman, W. J., de Villiers, M., and Strauss, E. (2014) Recent advances in targeting coenzyme A biosynthesis and utilization for antimicrobial drug development. *Biochem. Soc. Trans. 42*, 1080-6. DOI: 10.1042/BST20140131
12. Divo, A. A., Geary, T. G., Davis, N. L., and Jensen, J. B. (1985) Nutritional Requirements of *Plasmodium falciparum* in Culture. I. Exogenously Supplied Dialyzable Components Necessary for Continuous Growth. *J. Protozool. 32*, 59-64. DOI: 10.1111/j.1550-7408.1985.tb03013.x
13. Wrenger, C., Eschbach, M.-L., Müller, I. B., Laun, N. P., Begley, T. P., and Walter, R. D. (2006) Vitamin B1 de novo synthesis in the human malaria parasite *Plasmodium falciparum* depends on external provision of 4-amino-5-hydroxymethyl-2-methylpyrimidine. *Biol. Chem. 387*, 41-51. DOI: 10.1515/BC.2006.007
14. Saliba, K. J., and Kirk, K. (2001) H^+-coupled pantothenate transport in the intracellular malaria parasite. *J. Biol. Chem. 276*, 18115-18121. DOI: 10.1074/jbc.M010942200
15. Spry, C., van Schalkwyk, D. A., Strauss, E., and Saliba, K. J. (2010) Pantothenate utilization by *Plasmodium* as a target for antimalarial chemotherapy. *Infect. Disord. Drug Targets 10*, 200-16. DOI: 10.2174/187152610791163390
16. Saliba, K. J., Horner, H. A., and Kirk, K. (1998) Transport and metabolism of the essential vitamin pantothenic acid in human erythrocytes infected with the malaria parasite *Plasmodium falciparum*. *J. Biol. Chem. 273*, 10190-10195. DOI: 10.1074/jbc.273.17.10190
17. Spry, C., Chai, C. L., Kirk, K., and Saliba, K. J. (2005) A class of pantothenic acid analogs inhibits *Plasmodium falciparum* pantothenate kinase and represses the proliferation of malaria parasites. *Antimicrob. Agents Chemother. 49*, 4649-4657. DOI: 10.1128/AAC.49.11.4649-4657.2005
18. Lehane, A. M., Marchetti, R. V., Spry, C., van Schalkwyk, D. A., Teng, R., Kirk, K., and Saliba, K. J. (2007) Feedback Inhibition of Pantothenate Kinase Regulates Pantothenol Uptake by the Malaria Parasite. *J. Biol. Chem. 282*, 25395-25405. DOI: 10.1074/jbc.M704610200
19. Spry, C., Saliba, K. J., and Strauss, E. (2014) A miniaturized assay for measuring small molecule phosphorylation in the presence of complex matrices. *Anal. Biochem. 451*, 76-8. DOI: 10.1016/j.ab.2013.12.010
20. Howieson, V. M., Tran, E., Hoegl, A., Fam, H. L., Fu, J., Sivonen, K., Li, X. X., Auclair, K., and Saliba, K. J. (2016) Triazole Substitution of a Labile Amide Bond Stabilizes Pantothenamides and Improves Their Antiplasmodial Potency. *Antimicrob. Agents Chemother. 60*, 7146-7152. DOI: 10.1128/aac.01436-16
21. Ivey, R. A., Zhang, Y.-M., Virga, K. G., Hevener, K., Lee, R. E., Rock, C. O., Jackowski, S., and Park, H.-W. (2004) The Structure of the Pantothenate Kinase·ADP·Pantothenate Ternary Complex Reveals the Relationship between the Binding Sites for Substrate, Allosteric Regulator, and Antimetabolites. *J. Biol. Chem. 279*, 35622-35629. DOI: 10.1074/jbc.M403152200
22. Leonardi, R., Chohnan, S., Zhang, Y.-M., Virga, K. G., Lee, R. E., Rock, C. O., and Jackowski, S. (2005) A pantothenate kinase from *Staphylococcus aureus* refractory to

feedback regulation by coenzyme A. *J. Biol. Chem. 280*, 3314-3322. DOI: 10.1074/jbc.M411608200

23. Virga, K. G., Zhang, Y.-M., Leonardi, R., Ivey, R. A., Hevener, K., Park, H.-W., Jackowski, S., Rock, C. O., and Lee, R. E. (2006) Structure-activity relationships and enzyme inhibition of pantothenamide-type pantothenate kinase inhibitors. *Bioorg. Med. Chem. 14*, 1007-1020. DOI: 10.1016/j.bmc.2005.09.021
24. Mercer, A. C., Meier, J. L., Hur, G. H., Smith, A. R., and Burkart, M. D. (2008) Antibiotic evaluation and in vivo analysis of alkynyl Coenzyme A antimetabolites in *Escherichia coli*. *Bioorg. Med. Chem. Lett. 18*, 5991-5994. DOI: 10.1016/j.bmcl.2008.07.078
25. Awuah, E., Ma, E., Hoegl, A., Vong, K., Habib, E., and Auclair, K. (2014) Exploring structural motifs necessary for substrate binding in the active site of *Escherichia coli* pantothenate kinase. *Bioorg. Med. Chem. 22*, 3083-3090. DOI: 10.1016/j.bmc.2014.04.030
26. Strauss, E., Coenzyme A Biosynthesis and Enzymology. In *Comprehensive Natural Products II Chemistry and Biology*, Mander, L.; Liu, H.-W., Eds. Elsevier: Oxford, 2010; Vol. 7, pp 351-410. DOI: 10.1016/B978-008045382-8.00141-6.
27. de Villiers, M., Barnard, L., Koekemoer, L., Snoep, J. L., and Strauss, E. (2014) Variation in pantothenate kinase type determines the pantothenamide mode of action and impacts on coenzyme A salvage biosynthesis. *FEBS J. 281*, 4731-53. DOI: 10.1111/febs.13013
28. Strauss, E., and Begley, T. P. (2002) The antibiotic activity of *N*-pentylpantothenamide results from its conversion to ethyldethia-coenzyme A, a coenzyme A antimetabolite. *J. Biol. Chem. 277*, 48205-48209. DOI: 10.1074/jbc.M204560200
29. Akinnusi, T. O., Vong, K., and Auclair, K. (2011) Geminal dialkyl derivatives of *N*-substituted pantothenamides: Synthesis and antibacterial activity. *Bioorg. Med. Chem. 19*, 2696-2706. DOI: 10.1016/j.bmc.2011.02.053
30. Zhang, Y.-M., Frank, M. W., Virga, K. G., Lee, R. E., Rock, C. O., and Jackowski, S. (2004) Acyl carrier protein is a cellular target for the antibacterial action of the pantothenamide class of pantothenate antimetabolites. *J. Biol. Chem. 279*, 50969-50975. DOI: 10.1074/jbc.M409607200
31. Thomas, J., and Cronan, J. E. (2010) Antibacterial activity of *N*-pentylpantothenamide is due to inhibition of coenzyme A synthesis. *Antimicrob. Agents Chemother. 54*, 1374-1377. DOI: 10.1128/AAC.01473-09
32. Mercer, A. C., and Burkart, M. D. (2007) The ubiquitous carrier protein—a window to metabolite biosynthesis. *Nat. Prod. Rep. 24*, 750-773. DOI: 10.1039/B603921A
33. Hughes, S. J., Barnard, L., Mottaghi, K., Tempel, W., Antoshchenko, T., Hong, B. S., Allali-Hassani, A., Smil, D., Vedadi, M., Strauss, E., and Park, H. W. (2016) Discovery of Potent Pantothenamide Inhibitors of *Staphylococcus aureus* Pantothenate Kinase through a Minimal SAR Study: Inhibition Is Due to Trapping of the Product. *ACS Infect. Dis. 2*, 627-641. DOI: 10.1021/acsinfecdis.6b00090
34. van Wyk, M., and Strauss, E. (2008) Development of a method for the parallel synthesis and purification of N-substituted pantothenamides, known inhibitors of coenzyme A biosynthesis and utilization. *Org. Biomol. Chem. 6*, 4348-55. DOI: 10.1039/b811086g
35. Saliba, K. J., Ferru, I., and Kirk, K. (2005) Provitamin B_5 (pantothenol) inhibits growth of the intraerythrocytic malaria parasite. *Antimicrob. Agents Chemother. 49*, 632-637. DOI: 10.1128/aac.49.2.632-637.2005
36. Balibar, C. J., Hollis-Symynkywicz, M. F., and Tao, J. (2011) Pantethine Rescues Phosphopantothenoylcysteine Synthetase and Phosphopantothenoylcysteine Decarboxylase Deficiency in *Escherichia coli* but Not in *Pseudomonas aeruginosa*. *J. Bacteriol. 193*, 3304-3312. DOI: 10.1128/jb.00334-11
37. Subramanian, C., Yun, M.-K., Yao, J., Sharma, L. K., Lee, R. E., White, S. W., Jackowski, S., and Rock, C. O. (2016) Allosteric Regulation of Mammalian Pantothenate Kinase. *J. Biol. Chem. 291*, 22302-22314. DOI: 10.1074/jbc.M116.748061

38. Hughes, S. J., Antoshchenko, T., Kim, K. P., Smil, D., and Park, H.-W. (2014) Structural characterization of a new N-substituted pantothenamide bound to pantothenate kinases from *Klebsiella pneumoniae* and *Staphylococcus aureus*. *Proteins: Struct., Funct., Bioinf. 82*, 1542-1548. DOI: 10.1002/prot.24524
39. Sibon, O. C. M., and Strauss, E. (2016) Coenzyme A: to make it or uptake it? *Nat. Rev. Mol. Cell Biol. 17*, 605-606. DOI: 10.1038/nrm.2016.110
40. Srinivasan, B., Baratashvili, M., van der Zwaag, M., Kanon, B., Colombelli, C., Lambrechts, R. A., Schaap, O., Nollen, E. A., Podgorsek, A., Kosec, G., Petkovic, H., Hayflick, S., Tiranti, V., Reijngoud, D. J., Grzeschik, N. A., and Sibon, O. C. M. (2015) Extracellular 4'-phosphopantetheine is a source for intracellular coenzyme A synthesis. *Nat. Chem. Biol. 11*, 784-792. DOI: 10.1038/nchembio.1906
41. Hart, R. J., Cornillot, E., Abraham, A., Molina, E., Nation, C. S., Ben Mamoun, C., and Aly, A. S. I. (2016) Genetic Characterization of *Plasmodium* Putative Pantothenate Kinase Genes Reveals Their Essential Role in Malaria Parasite Transmission to the Mosquito. *Sci. Rep. 6*, 33518. DOI: 10.1038/srep33518
42. Srivastava, A., Creek, D. J., Evans, K. J., De Souza, D., Schofield, L., Müller, S., Barrett, M. P., McConville, M. J., and Waters, A. P. (2015) Host Reticulocytes Provide Metabolic Reservoirs That Can Be Exploited by Malaria Parasites. *PLOS Pathogens 11*, e1004882. DOI: 10.1371/journal.ppat.1004882
43. van der Westhuyzen, R., Hammons, J. C., Meier, J. L., Dahesh, S., Moolman, W. J., Pelly, S. C., Nizet, V., Burkart, M. D., and Strauss, E. (2012) The antibiotic CJ-15,801 is an antimetabolite that hijacks and then inhibits CoA biosynthesis. *Chem. Biol. 19*, 559-71. DOI: 10.1016/j.chembiol.2012.03.013
44. Kumar, P., Chhibber, M., and Surolia, A. (2007) How pantothenol intervenes in Coenzyme-A biosynthesis of *Mycobacterium tuberculosis*. *Biochem. Biophys. Res. Commun. 361*, 903-909. DOI: 10.1016/j.bbrc.2007.07.080
45. Saliba, K., and Kirk, K. (2005) CJ-15,801, a fungal natural product, inhibits the intraerythrocytic stage of *Plasmodium falciparum in vitro* via an effect on pantothenic acid utilisation. *Mol. Biochem. Parasitol. 141*, 129-131. DOI: 10.1016/j.molbiopara.2005.02.003
46. Ke, H., Lewis, Ian A., Morrisey, Joanne M., McLean, Kyle J., Ganesan, Suresh M., Painter, Heather J., Mather, Michael W., Jacobs-Lorena, M., Llinás, M., and Vaidya, Akhil B. (2015) Genetic Investigation of Tricarboxylic Acid Metabolism during the *Plasmodium falciparum* Life Cycle. *Cell Rep. 11*, 164-174. DOI: 10.1016/j.celrep.2015.03.011
47. Vaughan, A. M., O'Neill, M. T., Tarun, A. S., Camargo, N., Phuong, T. M., Aly, A. S., Cowman, A. F., and Kappe, S. H. (2009) Type II fatty acid synthesis is essential only for malaria parasite late liver stage development. *Cell. Microbiol. 11*, 506-520. DOI: 10.1111/j.1462-5822.2008.01270.x
48. Yu, M., Kumar, T. R. S., Nkrumah, L. J., Coppi, A., Retzlaff, S., Li, C. D., Kelly, B. J., Moura, P. A., Lakshmanan, V., Freundlich, J. S., Valderramos, J.-C., Vilcheze, C., Siedner, M., Tsai, J. H. C., Falkard, B., Sidhu, A. b. S., Purcell, L. A., Gratraud, P., Kremer, L., Waters, A. P., Schiehser, G., Jacobus, D. P., Janse, C. J., Ager, A., Jacobs Jr, W. R., Sacchettini, J. C., Heussler, V., Sinnis, P., and Fidock, D. A. (2008) The fatty acid biosynthesis enzyme FabI plays a key role in the development of liver-stage malarial parasites. *Cell Host Microbe 4*, 567-578. DOI: 10.1016/j.chom.2008.11.001
49. Notredame, C., Higgins, D. G., and Heringa, J. (2000) T-coffee: a novel method for fast and accurate multiple sequence alignment. *J. Mol. Biol. 302*, 205-217. DOI: 10.1006/jmbi.2000.4042
50. Šali, A., and Blundell, T. L. (1993) Comparative Protein Modelling by Satisfaction of Spatial Restraints. *J. Mol. Biol. 234*, 779-815. DOI: 10.1006/jmbi.1993.1626
51. Friesner, R. A., Banks, J. L., Murphy, R. B., Halgren, T. A., Klicic, J. J., Mainz, D. T., Repasky, M. P., Knoll, E. H., Shelley, M., Perry, J. K., Shaw, D. E., Francis, P., and Shenkin, P. S. (2004) Glide: A New Approach for Rapid, Accurate Docking and Scoring. 1.

Method and Assessment of Docking Accuracy. *J. Med. Chem. 47*, 1739-1749. DOI: 10.1021/jm0306430

52. Shivakumar, D., Harder, E., Damm, W., Friesner, R. A., and Sherman, W. (2012) Improving the Prediction of Absolute Solvation Free Energies Using the Next Generation OPLS Force Field. *J. Chem. Theory Comput. 8*, 2553-2558. DOI: 10.1021/ct300203w
53. Jorgensen, W. L., and Tirado-Rives, J. (1988) The OPLS [optimized potentials for liquid simulations] potential functions for proteins, energy minimizations for crystals of cyclic peptides and crambin. *J. Am. Chem. Soc. 110*, 1657-1666. DOI: 10.1021/ja00214a001

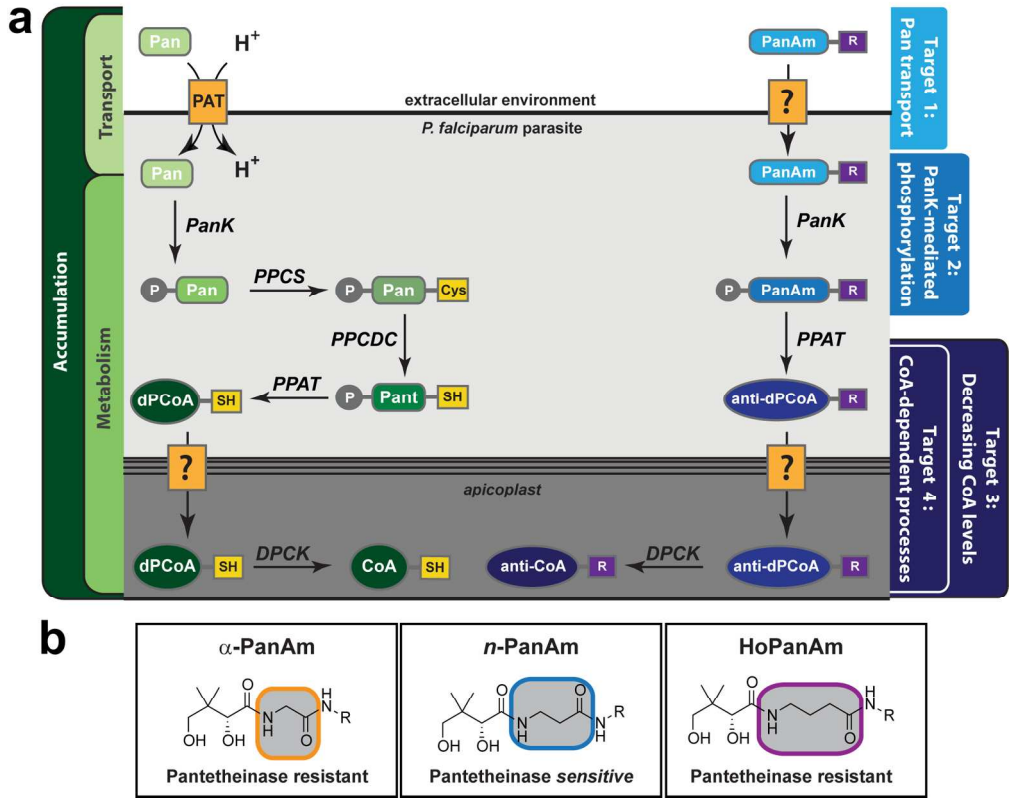

Figure 1. a) Biosynthesis of CoA in *P. falciparum*. Uptake of pantothenate (Pan) is followed by its biosynthetic conversion to CoA in a five-step pathway catalyzed by pantothenate kinase (PanK), phosphopantothenoylcysteine synthetase (PPCS), phosphopantothenoylcysteine decarboxylase (PPCDC), phosphopantetheine adenylyltransferase (PPAT), and finally dephospho-CoA kinase (DPCK), that produce 4'-phosphopantothenate (P-Pan), 4'-phosphopantothenoylcysteine (P-PanCys), 4'-phosphopantetheine (P-PantSH), 3'-dephospho-CoA (dPCoA) and CoA, respectively. The accumulation of Pan can be represented by the combined effects of the transport of the vitamin into the parasite and its metabolism by the CoA pathway starting with PanK-mediated phosphorylation. This ultimately leads to trapping of Pan within the parasite. Pantothenamides (shown as PanAm–R in the figure, with R denoting the amide substituent) can also be taken up by the parasite to exert their effect on CoA biosynthesis and/or utilization. PanAms are proposed to exert an antiplasmodial effect via one of four possible processes, or a combination thereof: 1) by inhibiting Pan transport, 2) by inhibiting PanK-mediated Pan phosphorylation, 3) by lowering CoA levels due to formation of CoA antimetabolites (anti-CoA) rather than CoA, and 4) by CoA antimetabolites interfering with CoA-dependent processes. **b)** PanAms that contain a β-alanine moiety (i.e. n-PanAms, middle) are susceptible to degradation by pantetheinase. Modification of the β-alanine moiety that displaces the scissile bond produces the α-PanAm (left) or HoPanAm (right) variants that are resistant to pantetheinase.[5]

159x127mm (300 x 300 DPI)

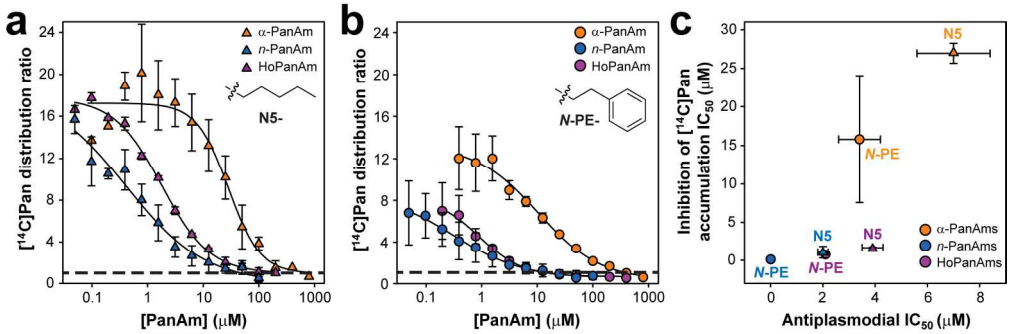

Figure 2. Effect of α-, *n*- and HoPanAms (N5 series in panel **a** and *N*-PE series in panel **b**, respectively) on [^{14}C]Pan accumulation (the combined effect of transport and metabolism) as measured by saponin-isolated *P. falciparum* trophozoites after 20 minutes. Accumulation decreases with increasing concentrations of the PanAms and reaches a distribution ratio of approximately one (indicated by a black dashed line). Accumulation data are an average of two separate experiments, each performed in duplicate. All error bars denote range/2. **c)** Correlation of the potency of inhibition of [^{14}C]Pan accumulation in isolated *P. falciparum* trophozoites by PanAms and the antiplasmodial potency obtained for PanAms against cultured blood-stage *P. falciparum* parasites. Antiplasmodial IC_{50} values were obtained from previous studies.[4,5] Error bars denote SEM or range/2 as appropriate for the particular data set.

176x59mm (300 x 300 DPI)

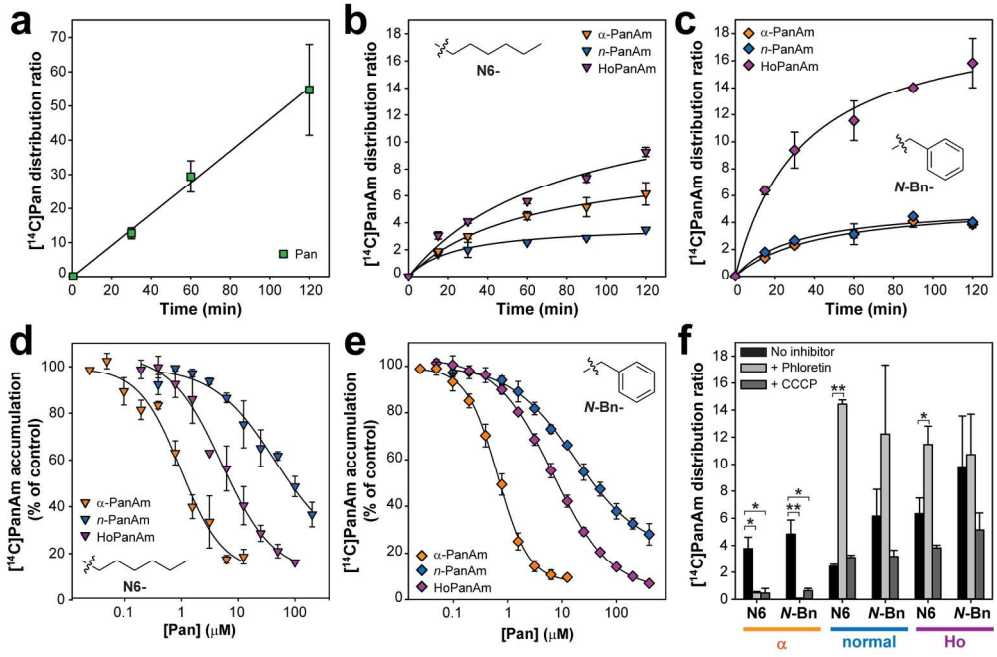

Figure 3. Accumulation of [^{14}C]Pan and [^{14}C]PanAm in saponin-isolated *P. falciparum* trophozoites. **a)** Accumulation of [^{14}C]Pan over 2 hours. Data represent an average of three separate experiments, each performed in duplicate and error bars denote SEM. **b)** Accumulation of the ^{14}C-labelled N6-series of PanAm variants over 2 hours. **c)** As for **b**, but for the ^{14}C-labelled *N*-Bn-series of PanAm variants. The data in panels **b** and **c** represent an average of two separate experiments, each performed in duplicate and error bars denote range/2. **d)** and **e)** Effect of increasing Pan concentration on [^{14}C]PanAm accumulation (panel **d** and **e** for the N6 and *N*-Bn series respectively) by saponin-isolated *P. falciparum* trophozoites after 60 minutes. Accumulation is plotted as percentage of a control with no Pan present. Both **d** and **e** represent an average of two separate experiments, each performed in duplicate and error bars denote range/2. **f)** Distribution ratio of both series of [^{14}C]PanAm variants after accumulation in isolated *P. falciparum* parasites for 30 minutes (indicated in black bars). Accumulation was also measured in the presence of 400 μM phloretin (light grey bars) and 10 μM CCCP (dark grey bars) for each compound under investigation. The data are an average of 2-4 separate experiments, each performed in duplicate and error bars denote SEM or range/2. Statistical analysis was done by performing an unpaired student's t-test (where * is $p < 0.05$ and ** is $p < 0.01$).

179x117mm (300 x 300 DPI)

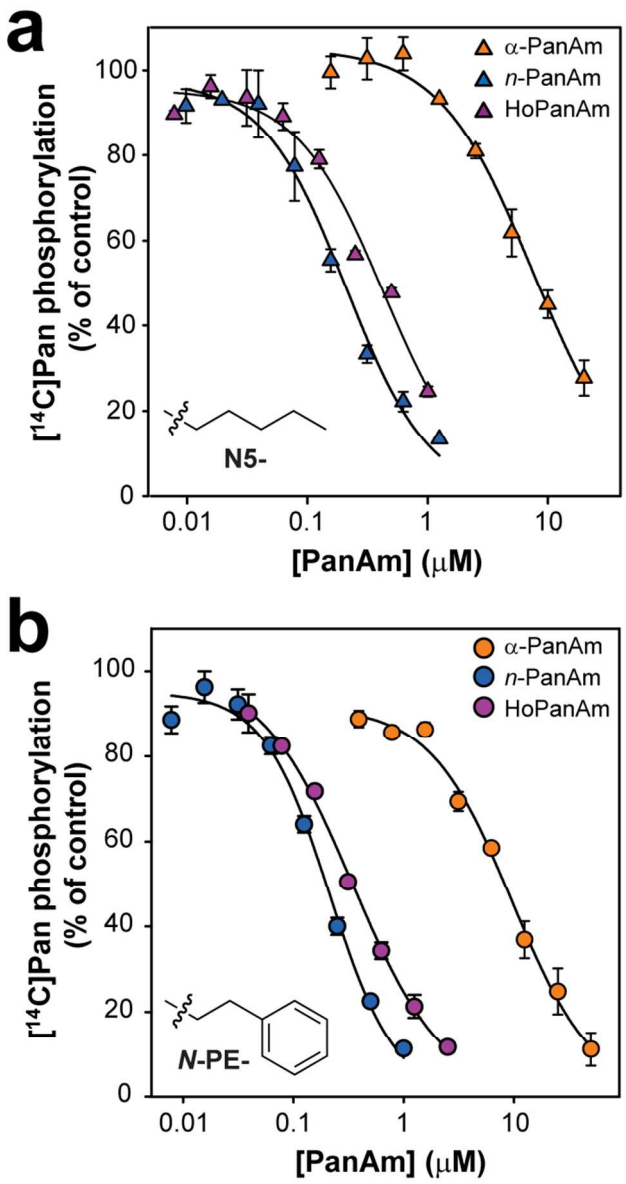

Figure 4. Inhibition of phosphorylation of 2 μM [^{14}C]Pan by *Pf*PanK present in parasite lysate by (**a**) N5- and (**b**) *N*-PE-substituted series of PanAm variants. Data were calculated as percentage of control reactions in which no PanAm was added (100% phosphorylation). For both panels **a** and **b** the data are an average of two separate experiments, each performed in duplicate; the error bars denote range/2.

65x117mm (300 x 300 DPI)

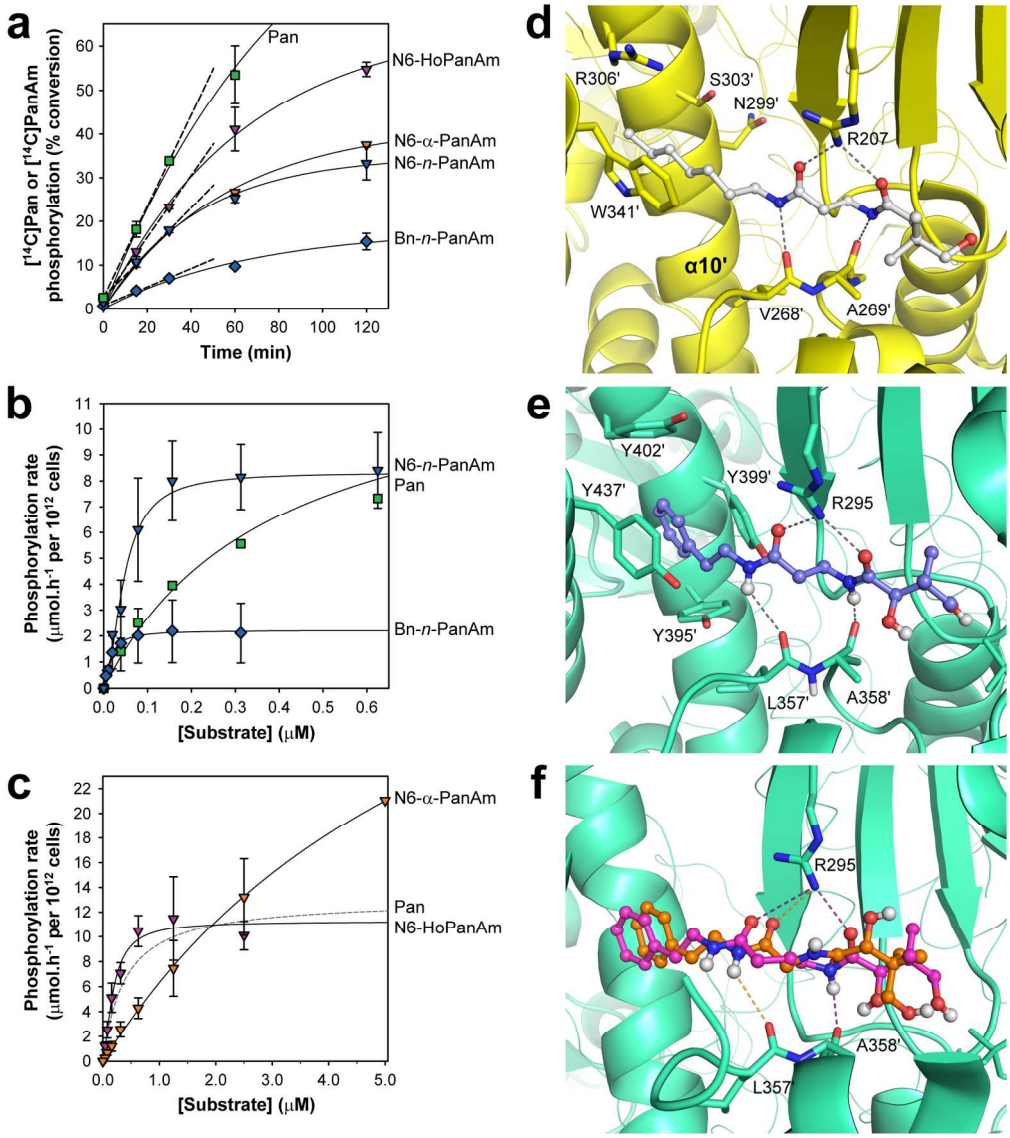

Figure 5. **a)** [^{14}C]PanAm phosphorylation by parasite lysate over 2 hours, shown as % conversion of total substrate added. Dashed lines indicate the linear portion of each curve, which is maintained over at least 30 min. The data are from one experiment performed in duplicate and error bars denote SD. **b)** Activity profiles of *Pf*PanK present in parasite lysate acting on [^{14}C]Pan, [^{14}C]N6- and [^{14}C]*N*-Bn-PanAm as substrates. **c)** Activity profiles of *Pf*PanK present in parasite lysate when supplied with increasing concentrations of [^{14}C]N6-α-PanAm or [^{14}C]N6-HoPanAm as substrates. The dashed line shows the Pan activity profile for reference. For both panels **b** and **c** the solid lines are the curves obtained from fitting either the Michaelis-Menten (for Pan and N6-α-PanAm) or Hill (for the *n*-PanAms and N6-HoPanAm) equations to the data. The data are an average of two separate experiments, each performed in duplicate and error bars denote range/2. **d)** Structure of HsPanK3 with N7-Pan (stick structure with C-atoms in white) bound in the active site (PDB id: 3SMS) showing the hydrogen bonding interactions with Arg207, which bridges the carbonyl oxygen atoms of the ligand's amide groups, as well as the hydrogen bonds between the backbone carbonyls of Val268' and Ala269' and the ligand's amide hydrogens. The four residues (N299', S303', R306' and W341') that are substituted for Tyr in *Pf*PanK are also indicated. **e)** Model of *Pf*PanK with *N*-PE-PanAm (stick structure with C-atoms in blue) bound showing the same hydrogen bonding interactions between the ligand and Arg295, Leu357' and Ala358'. The four Tyr residues (Tyr395', Tyr399', Tyr402' and Tyr437') that form

the hydrophobic pocket that accommodates the phenyl group of the ligand are indicated. **f)** The same model of *Pf*PanK showing the α-PanAm (stick structure with C-atoms in orange) and HoPanAm (stick structure with C-atoms in magenta) variants of *N*-PE-PanAm bound. In the case of *N*-PE-HoPanAm, only the interactions between Arg295 and the ligand's proximal amide group, and between the same amide N–H and the backbone carbonyl of Ala358' are maintained (indicated with magenta dashes), while the distance between Arg295 and its distal amide increases, leading to a weakened or lost interaction. In contrast, *N*-PE-α-PanAm maintains interactions (shown in orange dashes) between its distal amide and Arg295 and Leu357' respectively, as the proximal amide is rotated away. The rotation also leads to a very different placement of the geminal dimethyl groups as well as the 4'-OH group that is to be phosphorylated. The amide substituent is still accommodated in the pocket formed by the Tyr residues shown in panel **e**, but these were omitted for clarity.

161x183mm (300 x 300 DPI)

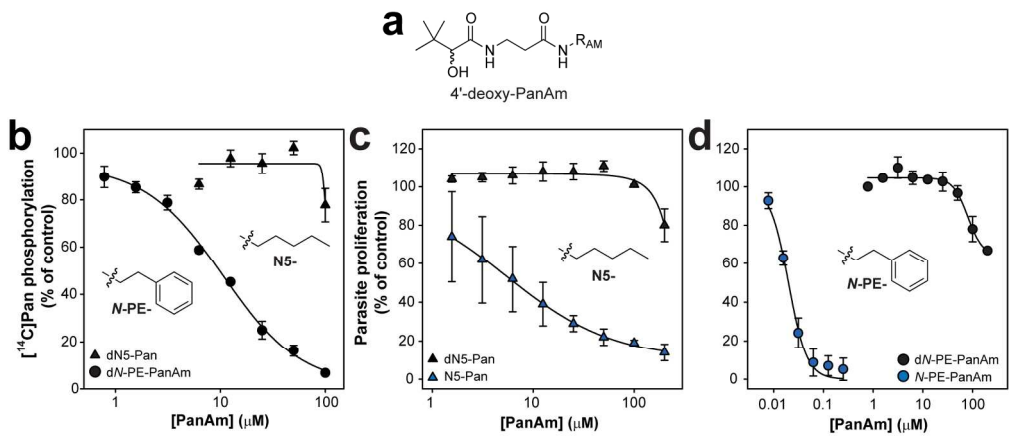

Figure 6. a) Chemical structure of DL-4'-deoxy-PanAms in which the 4'-OH-group of the parent compound is removed. **b)** Inhibition of phosphorylation of 2 μM [^{14}C]Pan by *Pf*PanK present in parasite lysate by dN5-Pan and d*N*-PE-PanAm. The data are an average of two separate experiments, each performed in duplicate; error bars denote range/2. **c)** and **d)** Antiplasmodial activity of N5-Pan (panel **c**) and *N*-PE-PanAm (panel **d**) in comparison to the corresponding deoxy variants of each compound in culture medium in which pantetheinase has been inactivated. Data for parent compounds are from previous published work.[4,5] Data for the deoxy-variants are an average of two separate experiments, each performed in triplicate and error bars denote range/2.

177x77mm (300 x 300 DPI)

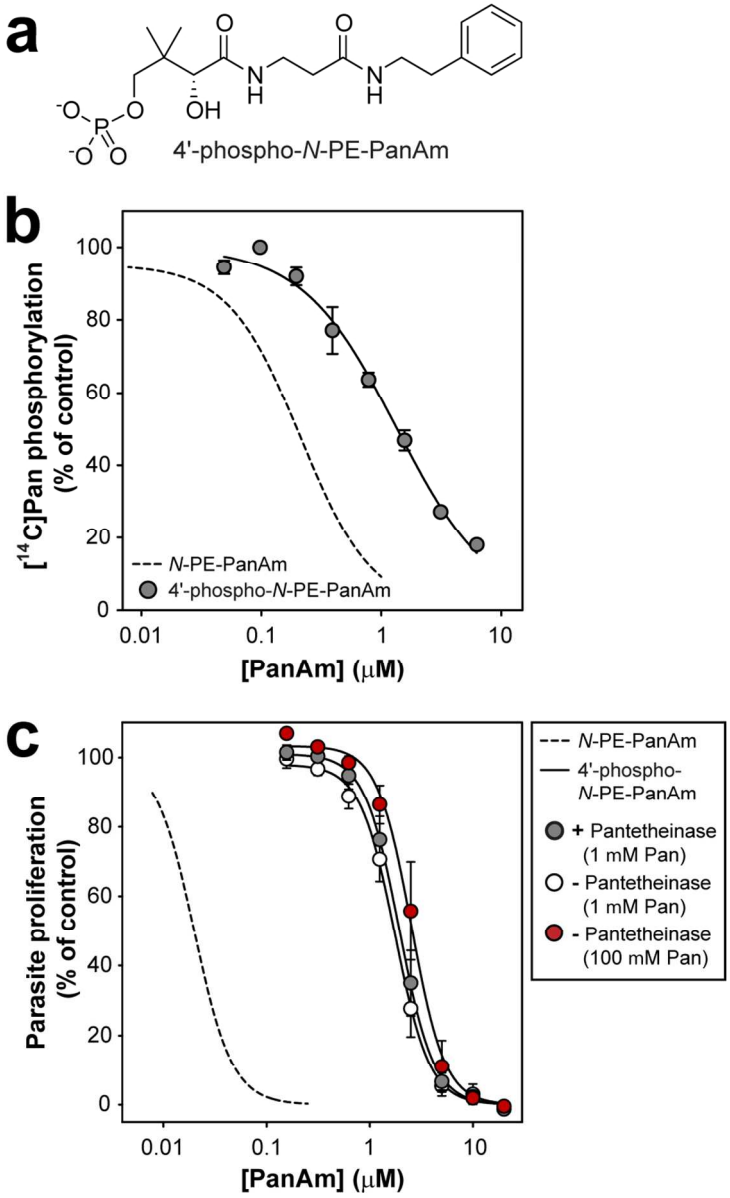

Figure 7. a) Chemical structure of 4'-phospho-*N*-PE-PanAm in which the 4'-OH-group of the parent compound is phosphorylated. **b)** 4'-Phospho-*N*-PE-PanAm-mediated inhibition of phosphorylation of 2 μM [^{14}C]Pan by *Pf*PanK present in parasite lysate. The data are an average of two separate experiments, each performed in duplicate and error bars denote range/2. The dotted line shows the fit for *N*-PE-PanAm-mediated inhibition (see Figure 4b) for comparison. **c)** Antiplasmodial activity of 4'-phospho-*N*-PE-PanAm in culture medium containing 1 μM Pan with and without pantetheinase activity. Activity was also measured in medium containing 100 μM Pan without pantetheinase activity. All data are an average of 3–4 separate experiments, each performed in triplicate; error bars denote SEM. The dotted line shows the fit for *N*-PE-PanAm-mediated inhibition (see Figure 6d) for comparison.

83x138mm (300 x 300 DPI)

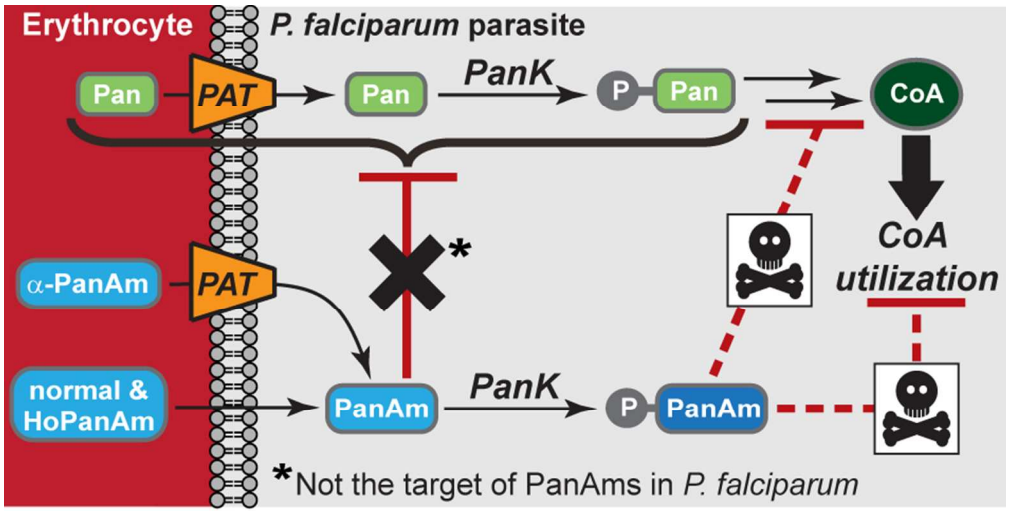

TOC Graphic

80x40mm (300 x 300 DPI)